

STATUS: arXiv pre-print

# A numerical method for scattering problems with unbounded interfaces

Tristan Goodwill  
*Department of Statistics and CCAM*  
*University of Chicago*  
*Chicago, IL 60637*  
tgoodwill@uchicago.edu

Charles L. Epstein  
*Center for Computational Mathematics*  
*Flatiron Institute, Simons Foundation*  
*New York, NY 10010*  
cepstein@flatironinstitute.org

November 19, 2024

# Abstract

We introduce a new class of computationally tractable scattering problems in unbounded domains, which we call *decomposable problems*. In these decomposable problems, the computational domain can be split into a finite collection of subdomains in which the scatterer has a “simple” structure. A subdomain is simple if the domain Green’s function for this subdomain is either available analytically or can be computed numerically with arbitrary accuracy by a tractable method. These domain Green’s functions are then used to reformulate the scattering problem as a system of boundary integral equations on the union of the subdomain boundaries. This reformulation gives a practical numerical method, as the resulting integral equations can then be solved, to any desired degree of accuracy, by using coordinate complexification over a *finite* interval, and standard discretization techniques.

AMS subject classifications: 35C15, 35Q60, 65M80, 65R20, 65E05

## Contents

<b>1</b>	<b>Introduction</b>	<b>2</b>
<b>2</b>	<b>Review of Matched Wave-guides</b>	<b>8</b>
2.1	Wave-guide modes . . . . .	8
2.2	IE for matched Wave-guides . . . . .	9
2.3	Asymptotics of Solutions and the Scattering Matrix . . . . .	11
<b>3</b>	<b>Green’s function for a single wave-guide</b>	<b>13</b>
3.1	Integral equation formulation . . . . .	15
3.2	Discretization . . . . .	17
3.3	Numerical verification . . . . .	18
<b>4</b>	<b>Solving the matched IE</b>	<b>18</b>
4.1	Outgoing skeleton . . . . .	21
4.2	Incoming skeletons . . . . .	22
4.3	Far sources and far targets . . . . .	23
4.4	Far sources and near targets . . . . .	24
4.5	Near sources and far targets . . . . .	26
4.6	Near sources and near targets . . . . .	27
<b>5</b>	<b>Numerical experiments</b>	<b>28</b>
<b>6</b>	<b>The scattering matrix and radiated power</b>	<b>30</b>
6.1	Finding the wave-guide modes . . . . .	30
6.2	Energy calculations . . . . .	31

<b>7 Other examples</b>	<b>32</b>
7.1 Terminating wave-guides . . . . .	32
7.2 Bent Wave-guides . . . . .	34
7.3 A Wave-guide junction . . . . .	34
7.4 Dirichlet Wave-guides . . . . .	37
<b>8 Conclusion</b>	<b>39</b>
<b>A Energy Conservation for Open Wave-guides</b>	<b>40</b>
<b>B Representation of Solutions Near to Channel Ends</b>	<b>45</b>

# 1 Introduction

There are many circumstances where one would like to examine how waves scatter off of unbounded interfaces. In this paper we consider only scalar waves described as perturbations of the Helmholtz equation. A typical unbounded scatterer is a network of open wave-guides described by  $\Delta + q(\mathbf{x}) + k^2$  where the potential is of the form

$$q(\mathbf{x}) = q_0(\mathbf{x}) + \sum_{j=1}^N q_j(\mathbf{x} - \langle \mathbf{x}, \omega_j \rangle \omega_j) \chi_{[1, \infty)}(r_j \langle \mathbf{x}, \omega_j \rangle). \quad (1.1)$$

Here  $q_0$  is a compactly supported function, the  $\{q_j : j = 1, N\}$  are compactly supported functions of one fewer variable, the  $\{\omega_j\}$  are distinct unit vectors, and the  $\{r_j\}$  are positive numbers. A schematic example is shown in Figure 1.

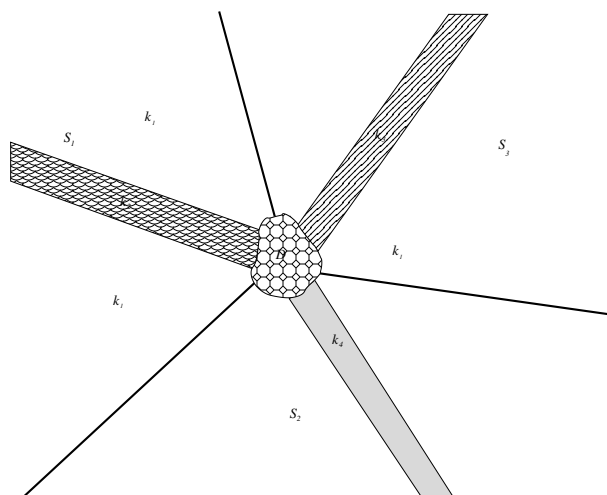


Figure 1: Three dielectric channels meeting in a compact interaction zone,  $D$ , showing sectors  $S_1, S_2, S_3$ .

Another situation where such interfaces arise is that of a half space with either a potential supported near the boundary, or perhaps a boundary that is itself non-flat over a non-compact set, see Figure 2. Problems of this sort have proved quite resistant to accurate numerical solution.

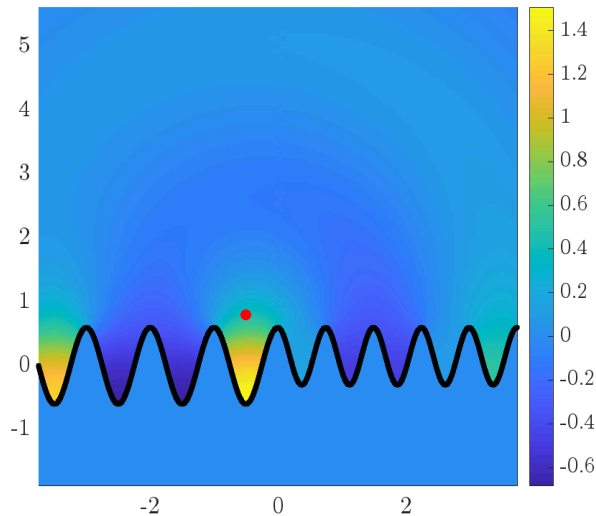


Figure 2: Two semi-infinite periodic boundaries meeting at along a common perpendicular line.

Methods for this class of problem can be placed into one of a few categories. Many use approximations to truncate the domain [4, 9, 21, 24, 26, 27, 29, 34, 39, 48]. Of particular interest is the method described in [11], which converge superalgebraically with truncation length. There also exist methods based on time domain calculations [2, 32, 40], or are restricted to the case where (1.1) is a perturbation of a layered media problem [12, 13, 33, 36, 37, 42, 45, 49]. There also exist a few methods that have solved the problem by imposing artificial radiation conditions [8, 35]. In this and subsequent papers in this series, we present a new approach to the numerical solution of a certain subclass of such problems. This method has been shown to give the unique solution of the problem with physically meaningful radiation conditions and gives provably exponentially small truncation error. Further, the reformulated method can easily be discretized using standard integral equation techniques.

We let  $L = \Delta + q(\mathbf{x})$ ; the scattering problem is to find an “outgoing” solution to

$$(L + k^2)u = f, \tag{1.2}$$

where  $f$  is defined by “incoming data.” The precise formulation of incoming and outgoing radiation conditions depends on the problem at hand. The operator  $L$  is usually self-adjoint so that the resolvent operator  $(L + k^2 + i\delta)^{-1}$  is a bounded operator on  $L^2$  provided that  $\delta \neq 0$ . The limiting absorption principle

then states that the limits

$$(L + k^2 \pm i0)^{-1} = \lim_{\delta \rightarrow 0^\pm} (L + k^2 + i\delta)^{-1} \quad (1.3)$$

exist as bounded operators between weighted spaces, e.g. as a bounded maps

$$(L + k^2 \pm i0)^{-1} : (1 + |\mathbf{x}|^2)^{-\frac{1+\eta}{4}} L^2(\mathbb{R}^d) \longrightarrow (1 + |\mathbf{x}|^2)^{\frac{1+\eta}{4}} L^2(\mathbb{R}^d),$$

for any  $\eta > 0$ , see [44]. If  $f$  is compactly supported, then  $u^+ = (L + k^2 + i0)^{-1} f$  is typically the unique outgoing solution to  $(L + k^2)u^+ = f$ . The long-range nature of the potential and the existence of wave-guide modes make it much more complicated to state the radiations conditions, and check that they imply uniqueness. Physically motivated radiated conditions in  $d$ -dimensions, implying uniqueness for potentials like those in (1.1), are given in [19].

If  $q(\mathbf{x}) = (k_1^2 - k^2)\chi_D(\mathbf{x})$ , for  $D$  a compact region with a smooth boundary, then the standard scattering problem is formulated as follows: We let  $v^{\text{inc}}$  be a solution to  $(\Delta + k^2)v^{\text{inc}} = 0$  in the exterior of  $D$ , smooth up to  $\partial D$ . We then look for functions  $u_\pm$  with

$$\begin{aligned} (\Delta + k^2)u_+(\mathbf{x}) &= 0 \text{ for } \mathbf{x} \in D^c, \\ (\Delta + k_1^2)u_-(\mathbf{x}) &= 0 \text{ for } \mathbf{x} \in D, \end{aligned} \quad (1.4)$$

and set

$$u^{\text{tot}}(\mathbf{x}) = \begin{cases} v^{\text{inc}}(\mathbf{x}) + u_+(\mathbf{x}) & \text{for } \mathbf{x} \in D^c, \\ u_-(\mathbf{x}) & \text{for } \mathbf{x} \in D. \end{cases} \quad (1.5)$$

In addition,  $u_+$  is required to satisfy the outgoing radiation condition, which in 2-dimensions means that

$$(\partial_r - ik)u_+(r\omega) = o(r^{-\frac{1}{2}}), \quad (1.6)$$

uniformly in  $\omega \in S^1$ . The solution is uniquely determined by the condition that  $u^{\text{tot}} \in H_{\text{loc}}^2(\mathbb{R}^2)$ , which is equivalent to the transmission boundary conditions

$$\begin{aligned} u_-(\mathbf{x}) - u_+(\mathbf{x}) &= v^{\text{inc}}(\mathbf{x}) \text{ for } \mathbf{x} \in \partial D, \\ \partial_{\mathbf{n}} u_-(\mathbf{x}) - \partial_{\mathbf{n}} u_+(\mathbf{x}) &= \partial_{\mathbf{n}} v^{\text{inc}}(\mathbf{x}) \text{ for } \mathbf{x} \in \partial D, \end{aligned} \quad (1.7)$$

here  $\mathbf{n}$  is the outer unit normal vector field to  $\partial D$ .

The standard method to solve this problem is to express  $u_\pm$  in terms of layer potentials on  $\partial D$ . The function

$$G_k(\mathbf{x}; \mathbf{y}) = \frac{i}{4\pi} H_0^{(1)}(k|\mathbf{x} - \mathbf{y}|), \quad (1.8)$$

is the outgoing fundamental solution for  $(\Delta + k^2)$ ; for  $\mathbf{x} \notin \partial D$ , we let

$$\begin{aligned} \mathcal{S}_k[\tau](\mathbf{x}) &= \int_{\partial D} G_k(\mathbf{x}; \mathbf{y}) \tau(\mathbf{y}) ds(\mathbf{y}) \\ \mathcal{D}_k[\sigma](\mathbf{x}) &= \int_{\partial D} \partial_{\mathbf{n}_y} G_k(\mathbf{x}; \mathbf{y}) \sigma(\mathbf{y}) ds(\mathbf{y}) \end{aligned} \quad (1.9)$$

denote the single and double layer potentials. Assume that

$$\begin{aligned} u_+(\mathbf{x}) &= \mathcal{S}_k[\tau](\mathbf{x}) + \mathcal{D}_k[\sigma](\mathbf{x}) \text{ for } \mathbf{x} \in D^c, \\ u_-(\mathbf{x}) &= \mathcal{S}_{k_1}[\tau](\mathbf{x}) + \mathcal{D}_{k_1}[\sigma](\mathbf{x}) \text{ for } \mathbf{x} \in D. \end{aligned} \quad (1.10)$$

Restricting  $u_{\pm}$  to the  $\partial D$  and using standard jump conditions for layer potentials we find that the conditions in (1.7) are equivalent to the system of integral equations

$$\begin{pmatrix} \text{Id} + K_1 & K_2 \\ K_3 & \text{Id} + K_4 \end{pmatrix} \begin{pmatrix} \sigma \\ \tau \end{pmatrix} = \begin{pmatrix} -v^{\text{inc}} \\ \partial_{\mathbf{n}} v^{\text{inc}} \end{pmatrix}, \quad (1.11)$$

where the  $\{K_j\}$  are compact operators acting on Hölder continuous functions on  $\partial D$ . As such these are Fredholm equations of second kind, and therefore generally well conditioned. By construction,  $u_+$  is an outgoing solution.

In this work, we adapt this method to obtain numerical solutions of scattering problems from non-compact scatterers. The principal idea is to geometrically decompose the problem into sub-problems for which the outgoing fundamental solutions can be efficiently approximated numerically. These fundamental solutions are no longer available in closed form, but require the solutions of non-trivial, but tractable, PDE problems. Cases where these sorts of more complicated Green's functions have been used include layered media with piecewise constant layers [12, 13, 33, 36, 42, 45, 49], and subsets of a halfspace with a periodic boundary [1]. Our approach to such scattering problems has three principal components.

1. Replace the scattering problem with a transmission problem.
  - (a) Divide space into a finite collection of half spaces, cylinders, and asymptotically conical sectors  $\{S_j : j = 1, \dots, N\}$ , along with a compact set  $S_0$  (see Figure 1). These subsets meet along piecewise smooth curves that lie on straight lines outside of a compact set.
  - (b) In each sector,  $S_j$ , the operator  $L$  agrees with an operator  $L_j$  for which we can numerically construct the kernel of the limiting absorption resolvent  $(L_j + k^2 + i0)^{-1}$ .
  - (c) In the subsets  $\{S_j : j = 1, \dots, N\}$  we express the solution as a sum of an incoming solution and an outgoing solution  $u_j = v_j^{\text{out}} + v_j^{\text{inc}}$  with  $(L_j + k^2)v_j^{\text{out}} = (L_j + k^2)v_j^{\text{inc}} = 0$ . The solutions  $\{v_j^{\text{inc}}\}$  are data encoding the incoming field. Each outgoing component  $v_j^{\text{out}}$  is expressed as a sum of layer potentials over the  $\partial S_j$  using the kernel of  $(L_j + k^2 + i0)^{-1}$  and its normal derivative
  - (d) The global solution is found by imposing transmission boundary conditions to ensure that the function defined by

$$u^{\text{tot}}(\mathbf{x}) = u_j(\mathbf{x}) \text{ for } \mathbf{x} \in S_j, j = 0, 1, \dots, N, \quad (1.12)$$

belongs to  $H_{\text{loc}}^2(\mathbb{R}^2)$ . This is the requirement the  $u_{\text{tot}}(\mathbf{x}), \nabla u_{\text{tot}}(\mathbf{x})$  are continuous, in the trace sense, across the boundaries of the sets  $\{\partial S_j : j = 0, \dots, N\}$ .

2. Using the integral representations,  $G_j(\mathbf{x}; \mathbf{y})$ , for  $(L_j + k^2 + i0)^{-1}$ , the transmission boundary conditions are re-expressed as systems of integral equations on  $\cup_j \partial S_j$ .
3. These integral equations are solved using the “coordinate complexification” method.

We call scatterers that satisfy 1(b) *decomposable*. The relationship between the data,  $\{v_j^{\text{inc}}\}$  and the data  $f$  in (1.2) depends on the problem one is solving. For example, if the incoming field comes from a point source,  $G_j(\mathbf{x}; \mathbf{y}_0)$  in  $S_j$ , then  $f$  would usually be defined by choosing a cut-off  $\psi$  equal 1 near to  $\mathbf{y}_0$  with support in  $S_j$ , and setting

$$f = (L_j + k^2)(\psi(\mathbf{x})G_j(\mathbf{x}; \mathbf{y}_0)). \quad (1.13)$$

The incoming data for the transmission problem is obtained by restricting  $G_j(\mathbf{x}; \mathbf{y}_0)$  and  $\partial_{\mathbf{n}_x} G_j(\mathbf{x}; \mathbf{y}_0)$  to  $\partial S_j$ . Similar considerations apply to other kinds of data, see [16]. In a series of papers, [16, 17, 19], it is *proved* that this method can be used to solve the scattering problem if the potential has the form

$$q(x_1, x_2) = q_l(x_2)\chi_{(-\infty, 0]}(x_1) + q_r(x_2)\chi_{[0, \infty)}(x_1). \quad (1.14)$$

In this paper we implement the method described above for this example, and show that it is also successful in much greater generality.

Key to the success of this program is the possibility of constructing kernels for the resolvents  $(L_j + k^2 + i0)^{-1}$ . In general, constructing these kernels may be a very difficult problem. However, if the potential has enough symmetry, then this construction often becomes a practically solvable problem. For example, let  $\mathbf{x} = (\mathbf{x}', \mathbf{x}'')$  be coordinates for  $\mathbb{R}^d$  and assume  $L = \Delta + q(\mathbf{x}')$ , where  $q$  is a compactly supported function of the  $\mathbf{x}'$ -variables. By taking Fourier transform in the remaining variables we obtain the operators

$$\tilde{L}[\xi''] = \Delta_{\mathbf{x}'} - |\xi''|^2 + q(\mathbf{x}'). \quad (1.15)$$

If  $q(\mathbf{x}')$  has compact support, then the explicit construction of  $(\tilde{L}[\xi''] + k^2 + i0)^{-1}$  can often be done quite efficiently. If  $|\xi''| > k$ , then  $(\tilde{L}[\xi''] + k^2)^{-1}$  is invertible, except possibly for  $|\xi''|$  in a finite set. The L.A.P. resolvent  $(L + k^2 + i0)^{-1}$  can then be constructed using Fourier synthesis. As the portions of the solutions corresponding to  $|\xi''| > k$  are largely evanescent, only frequencies in a compact set are required for numerical solutions with a specified accuracy. This approach to the construction of the L.A.P. resolvent has been used by many authors: for example it used for the case of layered media in [14, 38], and for the unreduced 2-body problem in [43]. Even having a discrete group of translational symmetries can make the construction of  $(L + k^2 + i0)^{-1}$  a computationally tractable problem, see [1].

In [29] a method for solving integral equations on infinite lines is introduced that we call the *complexification* method. This approach involves deforming the contour of integration into the complex plane, taking advantage of the fact

that the various fundamental solutions have analytic continuations to certain domains, and for some choices of incoming and outgoing variables, the analytically continued kernel functions are exponentially decaying. In [5, 6, 18, 41] similar methods are used to solve integral equations. This idea is quite similar to that used in the complex scaling method, as described in Chapter 4.5 of [15].

In order for the complexification method to work, it is necessary that the data also has analytic extension properties to appropriate domains, with exponential decay as functions of  $y_1 + iy_2$ . This is often the case for physically meaningful data. For example if we assume the integral equation is evaluated along the  $x_1$ -axis and take as incoming data the fundamental solution itself, with source off of this line, then, as  $y_1 \rightarrow \pm\infty$ , the function extends analytically to the sets  $Q_+ = \{(y_1 + it) : 0 < t, y_1\}$  and  $Q_- = \{(y_1 + it) : 0 > y_1, t\}$ . If  $a + ib$  belongs to one of these quadrants, then

$$H_0^{(1)}(k\sqrt{x_0^2 + (t(a + ib) - y_0)^2}) \sim \frac{e^{ikt(|a|+i|b|)}}{\sqrt{t(|a| + i|b|)}}[a_0 + O(t^{-1})], \quad (1.16)$$

decays exponentially. The square root is assumed to be defined on  $\mathbb{C} \setminus (-\infty, 0)$ , with positive values on  $(0, \infty)$ . As explained in [17], this implies that the solution to the integral equation has an asymptotic expansion, and the same analytic extension and exponential decay properties as the data and the kernel function. A simple example, with a rigorous analysis of the complexification method, is given in [18].

In Section 3 we use complexification to construct the L.A.P. resolvent kernel,  $G_q(\mathbf{x}; \mathbf{y})$ , in the case of a piece-wise constant, bi-infinite 2-dimensional waveguide. We suppose that the wave-guide lies in the region  $-d < x_2 < d$ , so that

$$q(x_2) = (k_1^2 - k^2)\chi_{\{|x_2| < d\}}(x_2). \quad (1.17)$$

In this case, we introduce the local wave-number

$$k(\mathbf{x}) = \begin{cases} k & \text{if } |x_2| > d, \\ k_1 & \text{if } |x_2| < d. \end{cases} \quad (1.18)$$

In each region we express the kernel as a perturbation of the appropriate free space fundamental solution,  $G_q(\mathbf{x}; \mathbf{y}) = G_{k(\mathbf{x})}(\mathbf{x}; \mathbf{y}) + G_q^{\text{out}}(\mathbf{x}; \mathbf{y})$ . The perturbation is found by using a boundary integral equation along  $\{x_2 = \pm d\}$  to solve for  $G_q^{\text{out}}$ , which is determined by transmission boundary conditions across the lines  $\{x_2 = \pm d\}$ , and the outgoing radiation condition. This method is explained in detail in Section 3. With these Green's functions in hand, one recasts the scattering problem as a transmission problem.

Most of this paper is devoted to a detailed description of this approach applied to potentials of the form given in (1.14). We explain the construction of the kernels of the limiting absorption resolvents  $(\Delta + q_{l,r}(x_1) + k^2 + i0)^{-1}$ . A practical construction was given in [16]; here we use a different method. We then set up the integral equations along the line  $\{x_1 = 0\}$ , and explain how to use complexification to solve this system of equations. This is followed by



many examples, which are solved using variants of our method. For scattering problems of this sort, one expects the incoming energy to equal the outgoing energy. We give a proof that this is the case for open wave guides in an Appendix. Computing these quantities, we show that our solutions have this property to many digits of accuracy.

While the method described above has only been rigorously justified for potentials of the form in (1.14), we show, in a series of examples, that the method actually provides accurate answers in more interesting and complicated geometries. These include, among others, semi-infinite wave guides with compact perturbations at the end, and a pair of open wave-guides meeting at various angles. These examples demonstrate the wider applicability of this approach.

### Acknowledgements

The authors would like to express our deep gratitude to Shidong Jiang for introducing us to the ideas underlying the complexification method, and encouraging us to use this approach to solve wave guide problems. We would also like to thank Jeremy Hoskins and Manas Rachh for their very important contributions to many aspects of this project. Finally, we would like to thank the American Institute of Mathematics and, in particular, John Fry for hosting us on Bock Cay during the SQuaREs program in May 2024. That meeting helped to launch this project in earnest.

## 2 Review of Matched Wave-guides

In this paper we first focus on the case of 2 semi-infinite wave-guides meeting along a common perpendicular line, which is the decomposable problem treated in [16]. This is modeled using a potential like that given in (1.14). For simplicity we consider the case of piecewise constant potentials,

$$q_{l,r}(x_2) = (k_{1;l,r}^2 - k^2)\chi_{[-d_{l,r}, d_{l,r}]}(x_2), \quad (2.1)$$

though the more general case of bounded piecewise, continuous potentials can also be handled using this method. We usually assume that the wave numbers,  $k_{1;l,r}$ , inside the channel are larger than that in the surrounding medium. This is needed for “wave-guide modes” to exist, and is the case of principal interest in opto-electronics.

### 2.1 Wave-guide modes

For an operator of this type there are finitely many solutions  $v_{l,r;n}(x_2) \in L^2(\mathbb{R})$  to

$$(\partial_{x_2}^2 + q_{l,r}(x_2))v_{l,r;n}(x_2) = \lambda_{l,r;n}^2 v_{l,r;n}(x_2), n = 1, \dots, N_{l,r}, \quad (2.2)$$

where  $0 < \lambda_{l,r;n}^2 < k_{1;l,r}^2 - k^2$ . In fact, such a solution is easily seen to be  $O(e^{-\lambda_{l,r;n}|x_2|})$  as  $|x_2| \rightarrow \infty$ . The frequencies for which such a solution exist can be found by solving a simple transcendental equation. If the channel has width

$2d$  with interior wave number  $k_{1;l,r}$ , and exterior wave number  $k$ , then the wave guide energies are found by solving

$$\tan 2d\sqrt{k_{1;l,r}^2 - k^2 - \lambda^2} = \frac{2\lambda\sqrt{k_{1;l,r}^2 - k^2 - \lambda^2}}{k_{1;l,r}^2 - k^2 - 2\lambda^2}. \quad (2.3)$$

If we let  $\xi_{l,r;n} = \sqrt{k^2 + \lambda_{l,r;n}^2} > 0$ , then we have that

$$(\Delta + q_{l,r} + k^2)e^{\pm i\xi_{l,r;n}x_1}v_{l,r;n}(x_2) = 0; \quad (2.4)$$

these are the *wave-guide modes*. They are not  $L^2$ -eigenfunctions in 2 dimensions as they do not decay in the  $x_1$ -direction, but they are strongly localized within the supp  $q_{l,r}$ . The functions

$$\{e^{i\xi_{l,r;n}x_1}v_{l,r;n}(x_2) : n = 1, \dots, N_{l,r}\} \quad (2.5)$$

are the rightward moving wave-guide modes and

$$\{e^{-i\xi_{l,r;n}x_1}v_{l,r;n}(x_2) : n = 1, \dots, N_{l,r}\} \quad (2.6)$$

are the leftward moving wave-guide modes.

As noted in our earlier work, two semi-infinite wave-guides meeting along a common perpendicular line is the simplest case for which it is not possible to explicitly compute the fundamental solution, and we instead follow the outline above and rephrase the scattering problem as a transmission problem along the common perpendicular line  $\{x_1 = 0\}$ . Typical incoming data for such a wave-guide structure is given by a sum of incoming wave-guide modes, i.e.

$$v_l^{\text{inc}} = \sum_{n=1}^{N_l} c_n e^{i\xi_{l,r;n}x_1}v_{l,r;n}(x_2), \text{ for } x_1 < 0, \quad (2.7)$$

though other types of incoming data are allowed, see Section 6 of [16]. The scattered field is a sum of outgoing wave-guide modes as well as outgoing radiation.

## 2.2 IE for matched Wave-guides

The first step in replacing the scattering problem with a transmission problem is the construction of outgoing fundamental solutions for the operators  $(\Delta + q_{l,r} + k^2)$ , whose kernels we denote by  $G_{q_{l,r}}(\mathbf{x}; \mathbf{y})$ . We assume that there are incoming fields  $v_{l,r}^{\text{inc}}$  defined in  $\pm x_1 > 0$ , which solve the equations

$$(\Delta + q_{l,r} + k^2)v_{l,r}^{\text{inc}} = 0 \text{ where } \pm x_1 > 0. \quad (2.8)$$

The total field is given by

$$u^{\text{tot}}(x_1, x_2) = \begin{cases} v_l^{\text{inc}}(x_1, x_2) + v_l^{\text{out}}(x_1, x_2) & \text{where } x_1 < 0, \\ v_r^{\text{inc}}(x_1, x_2) + v_r^{\text{out}}(x_1, x_2) & \text{where } x_1 > 0; \end{cases} \quad (2.9)$$

the  $v_{l,r}^{\text{out}}$  are “outgoing” solutions to  $(\Delta + q_{l,r} + k^2)v_{l,r}^{\text{out}} = 0$  where  $\pm x_1 > 0$ . These solutions are determined by the transmission boundary conditions

$$\begin{aligned} v_l^{\text{inc}}(0^-, x_2) + v_l^{\text{out}}(0^-, x_2) &= v_r^{\text{inc}}(0^+, x_2) + v_r^{\text{out}}(0^+, x_2) \\ \partial_{x_1} v_l^{\text{inc}}(0^-, x_2) + \partial_{x_1} v_l^{\text{out}}(0^-, x_2) &= \partial_{x_1} v_r^{\text{inc}}(0^+, x_2) + \partial_{x_1} v_r^{\text{out}}(0^+, x_2). \end{aligned} \quad (2.10)$$

Provisionally, the outgoing condition is imposed by representing  $v_{l,r}^{\text{out}}$  in terms of layer potentials constructed out of the outgoing fundamental solutions, for  $\pm x_1 > 0$ :

$$\begin{aligned} v_{l,r}^{\text{out}}(\mathbf{x}) &= \mathcal{S}_{q_{l,r}}[\tau](\mathbf{x}) + \mathcal{D}_{q_{l,r}}[\sigma](\mathbf{x}) \\ &= \int_{-\infty}^{\infty} G_{q_{l,r}}(\mathbf{x}; 0, y_2) \tau(y_2) dy_2 + \int_{-\infty}^{\infty} \partial_{y_1} G_{q_{l,r}}(\mathbf{x}; 0, y_2) \sigma(y_2) dy_2. \end{aligned} \quad (2.11)$$

As shown in [16, 17, 19], for appropriate incoming data, the functions  $v_{l,r}^{\text{out}}$  define solutions that satisfy the physically meaningful outgoing radiation conditions. The boundary conditions in (2.10) lead to integral equations along the line  $\{x_1 = 0\}$ ,

$$\begin{aligned} \lim_{x_1 \rightarrow 0^-} \left[ \int_{-\infty}^{\infty} (G_{q_l}(\mathbf{x}; 0, y_2) \tau(y_2) + \partial_{y_1} G_{q_l}(\mathbf{x}; 0, y_2) \sigma(y_2)) dy_2 \right] - \\ \lim_{x_1 \rightarrow 0^+} \left[ \int_{-\infty}^{\infty} (G_{q_r}(\mathbf{x}; 0, y_2) \tau(y_2) + \partial_{y_1} G_{q_r}(\mathbf{x}; 0, y_2) \sigma(y_2)) dy_2 \right] = \\ v_r^{\text{inc}}(0, x_2) - v_l^{\text{inc}}(0, x_2); \end{aligned} \quad (2.12)$$

$$\begin{aligned} \lim_{x_1 \rightarrow 0^-} \partial_{x_1} \left[ \int_{-\infty}^{\infty} (G_{q_l}(\mathbf{x}; 0, y_2) \tau(y_2) + \partial_{y_1} G_{q_l}(\mathbf{x}; 0, y_2) \sigma(y_2)) dy_2 \right] - \\ \lim_{x_1 \rightarrow 0^+} \partial_{x_1} \left[ \int_{-\infty}^{\infty} (G_{q_r}(\mathbf{x}; 0, y_2) \tau(y_2) + \partial_{y_1} G_{q_r}(\mathbf{x}; 0, y_2) \sigma(y_2)) dy_2 \right] = \\ \partial_{x_1} v_r^{\text{inc}}(0, x_2) - \partial_{x_1} v_l^{\text{inc}}(0, x_2) \end{aligned} \quad (2.13)$$

Using standard jump conditions for layer potentials, and a detailed analysis of the kernels  $G_{q_{l,r}}(\mathbf{x}; \mathbf{y})$  it is shown in [16] that these equations take the rather simple form

$$\begin{pmatrix} \text{Id} & D \\ C & \text{Id} \end{pmatrix} \begin{pmatrix} \sigma \\ \tau \end{pmatrix} = \begin{pmatrix} v_r^{\text{inc}}(0, x_2) - v_l^{\text{inc}}(0, x_2) \\ \partial_{x_1} [v_r^{\text{inc}}(0, x_2) - v_l^{\text{inc}}(0, x_2)] \end{pmatrix}. \quad (2.14)$$

The operator on the left hand side is a Fredholm operator of index zero acting on the spaces  $\mathcal{C}_\alpha(\mathbb{R}) \oplus \mathcal{C}_{\alpha+\frac{1}{2}}(\mathbb{R})$  for  $0 < \alpha < \frac{1}{2}$  of weighted continuous functions. The norm on  $\mathcal{C}_\beta(\mathbb{R})$  is defined by

$$|f|_\beta = \sup\{(1 + |x|)^\beta |f(x)| : x \in \mathbb{R}\}. \quad (2.15)$$

In [19] it is shown that the null spaces of these equations are trivial. This shows that these equations are uniquely solvable for arbitrary data  $(g, h) \in \mathcal{C}_\alpha(\mathbb{R}) \oplus \mathcal{C}_{\alpha+\frac{1}{2}}(\mathbb{R})$ . In order for the corresponding solution to the transmission problem to satisfy the physically meaningful radiation conditions given in [19], the data must also satisfy appropriate radiation conditions.

In the following sections we give numerical approximations for the kernels of  $C$  and  $D$ ; in [46] we show that they continue analytically to certain subsets of  $\mathbb{C} \times \mathbb{C}$ . For data  $(g, h)$  that also has analytic continuations we can deform the contour on which we are solving the integral equation. The analytic continuations of the data and the solutions  $(\sigma, \tau)$  are exponentially decaying. This allows us to solve the integral equations for  $\{(\sigma(x_2), \tau(x_2)) : x_2 \in [-L, L]\}$ , for any fixed  $L > 0$  and with any specified accuracy, by replacing the infinite domain implicit in (2.14) with a finite interval on the deformed contour. See the end of Section 3.1.

### 2.3 Asymptotics of Solutions and the Scattering Matrix

Of special interest in problems connected to open wave-guides is the scattering matrix, which relates the leading incoming part of the solution to the leading outgoing part. Suppose  $u$  is a solution to  $(\Delta + q + k^2)u = 0$ , where  $q$  is a potential of the type defined in (1.1). Let  $S^1$  be identified with the boundary of the radial compactification of  $\mathbb{R}^2$ , with  $\{\omega_1, \dots, \omega_N\}$  the endpoints of the channels at infinity. Assume that  $u$  has an asymptotic expansion at infinity of the form

$$u(r\omega) \sim \frac{e^{ikr}}{\sqrt{r}} a_+(\omega) + \frac{e^{-ikr}}{\sqrt{r}} a_-(\omega) + o(r^{-\frac{1}{2}}). \quad (2.16)$$

The coefficients  $a_\pm \in L^\infty(S^1)$  are smooth, functions on  $S^1 \setminus \{\omega_1, \dots, \omega_N\}$ .

Along the channels,  $u$  satisfies:

$$u(\mathbf{x}) = \sum_{n=1}^{M_j} [a_n^j e^{i\xi_n^j \langle \mathbf{x}, \omega_j \rangle} + b_n^j e^{-i\xi_n^j \langle \mathbf{x}, \omega_j \rangle}] v_n^j(\langle \mathbf{x}, \omega_j^\perp \rangle) + O(|\langle \mathbf{x}, \omega_j \rangle|^{-\frac{1}{2}}), \quad (2.17)$$

with  $\langle \omega_j, \omega_j^\perp \rangle = 0$  and  $\det(\omega_j, \omega_j^\perp) = 1$ . As shown in [19], this is true of solutions with a purely radial scattering wave-front set. The scattering matrix relating the incoming asymptotics to the outgoing asymptotics is defined by

$$S(k) : \left( \sqrt{k} a_-(\omega), \left[ \sqrt{\xi_n^j} b_n^j : n = 1, \dots, M_j, j = 1, \dots, N \right] \right) \mapsto \left( \sqrt{k} a_+(\omega), \left[ \sqrt{\xi_n^j} a_n^j : l = 1, \dots, M_j, j = 1, \dots, N \right] \right). \quad (2.18)$$

In Appendix A we prove the following conservation law, which is equivalent to the unitarity of the scattering matrix.

**Theorem 1.** *If  $u$  is solution to  $(\Delta + q + k^2)u = 0$ , with asymptotic expansions like those in (2.16) and (2.17), then*

$$k \int_{S^1} |a_-(\omega)|^2 d\omega + \sum_{j=1}^N \sum_{n=1}^{M_j} \xi_n^j |b_n^j|^2 = k \int_{S^1} |a_+(\omega)|^2 d\omega + \sum_{j=1}^N \sum_{n=1}^{M_j} \xi_n^j |a_n^j|^2. \quad (2.19)$$

In our applications, the only incoming part of the solution comes from the data, and we construct an outgoing solution  $u^{\text{out}}$ . In the proof of Theorem 1 we show that

$$\lim_{R \rightarrow \infty} \Im \left[ \int_0^{2\pi} \overline{u^{\text{out}}(R\omega)} \partial_r u^{\text{out}}(R\omega) R d\omega \right] = k \int_{S^1} |a_+(\omega)|^2 d\omega + \sum_{n=1}^{M_j} \xi_n^j |a_n^j|^2. \quad (2.20)$$

In [19] we also show that the coefficients  $\{|a_n^j|\}$  can also be found by computing the limits

$$|a_n^j| = \lim_{x_1 \rightarrow \infty} \left| \int_{-\infty}^{\infty} u^{\text{out}}(x_1, x_2) v_n^j(x_2) dx_2 \right|. \quad (2.21)$$

In [16] we show that for the special case of 2 semi-infinite wave guides meeting along a common perpendicular line

$$\begin{aligned} a_n^r e^{i\xi_n^r x_1} &= \int_{-\infty}^{\infty} v_r^{\text{out}}(x_1, x_2) v_n^r(x_2) dx_2 \text{ for any } x_1 > 0, \\ a_n^l e^{-i\xi_n^l x_1} &= \int_{-\infty}^{\infty} v_l^{\text{out}}(x_1, x_2) v_n^l(x_2) dx_2 \text{ for any } x_1 < 0. \end{aligned} \quad (2.22)$$

The solutions we construct to the scattering problem certainly satisfy the PDE everywhere, and belong to  $H_{\text{loc}}^2(\mathbb{R}^2)$ . The only real question is whether the solutions we construct are truly outgoing. As there is essentially no data for which there is a gold standard for numerical solutions of open wave guide scattering problems, these observations give a useful way to assess the quality of the solutions found by a numerical algorithm. The left hand side of (2.19) is computable from the incoming field, which is specified as data. Equations (2.20)–(2.22) provide a computationally effective means to approximate the right hand side of (2.19). While a very small difference between the two sides does not prove the pointwise accuracy of a solution, it does provide strong evidence that the solution we obtain satisfies the outgoing radiation condition.

From (2.16) we also see that the computed solution  $u^{\text{out}}$  has an expansion

$$\frac{R}{k} \overline{u^{\text{out}}(R\omega)} \partial_r u^{\text{out}}(R\omega) = i[|a_+(\omega)|^2 - |a_-(\omega)|^2] - 2\Im[e^{2ikR} a_+(\omega) \overline{a_-(\omega)}] + O(R^{-1}), \quad (2.23)$$

provided  $\omega \notin \{\omega_1, \dots, \omega_N\}$ . Evaluating this for a large  $R$  gives a pointwise estimate on the failure of the solution to be outgoing. In particular, we should find that

$$\Re \overline{u^{\text{out}}(R\omega)} \partial_r u^{\text{out}}(R\omega) = O(R^{-2}).$$

### 3 Green's function for a single wave-guide

In order to solve (2.14) we must be able to compute a bi-infinite wave-guide Green's function. There is a vast literature on this subject (see, for example [11–13, 33, 36, 42, 45, 49]). One popular method is to compute the inverse Fourier transform of the L.A.P. resolvent kernels of  $\partial_{x_2} - \xi^2 + k^2 + q(x_2)$ . The resulting formulas are also referred to as Sommerfeld integral formulas and are used in [13, 33, 36, 45, 49]. An alternative approach is the windowed Green's function approach developed in [11, 12]. In this section, we briefly present a new method based on the coordinate complexification technique developed in [18]. Indeed, any method may be used to find the Green's function without changing the subsequent steps needed to solve the scattering problem. We choose this method so that we can use the same discretization techniques in (3.12), (2.14) and the other integral equations in Section 7.

In this paper we consider piece-wise constant wave-guides, which corresponds to the choice of  $q(x_2) = (k_1^2 - k^2)\chi_{[-d,d]}(x_2)$ . As we mentioned in the introduction, we write a bi-infinite wave-guide Green's function as  $G_q(\mathbf{x}; \mathbf{y}) = G_{k(\mathbf{x})}(\mathbf{x}; \mathbf{y}) + G_q^{\text{out}}(\mathbf{x}; \mathbf{y})$ . It is not hard to see that  $G_q^{\text{out}}$  is the “outgoing” solution of the transmission problem

$$\begin{cases} (\Delta + k^2 + q(x_2))G_q^{\text{out}}(\mathbf{x}; \mathbf{y}) = 0 & \text{in } \mathbb{R}^2 \setminus \{|x_2| = d\}, \\ [[G_q^{\text{out}}]]_{|x_2|=d} = -[[G_{k(\mathbf{x})}]]_{|x_2|=d}, \\ [[\partial_{x_2} G_q^{\text{out}}]]_{|x_2|=d} = -[[\partial_{x_2} G_{k(\mathbf{x})}]]_{|x_2|=d}. \end{cases} \quad (3.1)$$

To numerically solve for  $G_q$ , it is therefore enough to be able solve transmission problems of this form. In the remainder of this section we discuss a numerical solver for transmission problems of this type. The decomposition used here differs from that in [16, 17] where we write  $G_q(\mathbf{x}; \mathbf{y}) = G_k(\mathbf{x}; \mathbf{y}) + \tilde{G}_q^{\text{out}}(\mathbf{x}; \mathbf{y})$ .

Before we do, however, we observe that this decomposition can easily be used to compute derivatives of  $G_q$ : the derivatives of  $G_{k(\mathbf{x})}$  can easily be computed and the derivatives of  $G_q^{\text{out}}$  can be computed by differentiating the solution or the boundary data of (3.1).

We finish this preliminary discussion by showing how the Sommerfeld integral representation leads to a solution, in principle, to this problem that clarifies how such a representation “finds” the correct wave-guide modes. In our actual computations we do not use the Fourier representation, but it becomes clearer why this approach works. We begin with the fact that the outgoing fundamental solution is obtained as the  $\lim_{\delta \rightarrow 0^+} (\Delta + k^2(x_2) + i\delta)^{-1}$ , and the Sommerfeld integral representation for the free space fundamental solution

$$G_{\sqrt{k^2+i\delta}}(\mathbf{x}; \mathbf{y}) = \frac{i}{4\pi} \int_{-\infty}^{\infty} \frac{e^{i|x_2-y_2|\sqrt{k^2+i\delta-\xi^2}} e^{i(x_1-y_1)\xi} d\xi}{\sqrt{k^2+i\delta-\xi^2}}. \quad (3.2)$$

Assume that the pole of  $G_{\sqrt{k^2+i\delta}}$  is  $\mathbf{y} = (0, y_2)$ , where  $y_2 > d$ ; similar considerations apply in all cases. We write the kernel,  $R_\delta(\mathbf{x}; \mathbf{y})$ , for  $(\Delta + k(x_2)^2 + i\delta)^{-1}$

as

$$R_\delta(\mathbf{x}; \mathbf{y}) = G_{\sqrt{k^2+i\delta}}(\mathbf{x}; \mathbf{y}) \cdot \chi_{[d,\infty)}(x_2) + e_\delta(\mathbf{x}; \mathbf{y}).$$

The correction term,  $e_\delta$  satisfies  $(\Delta_{\mathbf{x}} + k(x_2)^2 + i\delta)e_\delta = 0$  in the complement of the lines  $\{x_2 = \pm d\}$ , and is determined by transmission boundary conditions across these lines.

In each of the three regions we can express  $e_\delta$  as sums of single and double layer potentials:

$$\begin{aligned} e_\delta(\mathbf{x}; \mathbf{y}) &= \\ &\int_{-\infty}^{\infty} [G_{\sqrt{k^2+i\delta}}(\mathbf{x}; t, \pm d)\tau_\delta^\pm(t) \mp \partial_{y_2} G_{\sqrt{k^2+i\delta}}(\mathbf{x}; t, \pm d)\sigma_\delta^\pm(t)] dt, \text{ for } \pm x_2 > d, \\ e_\delta(\mathbf{x}; \mathbf{y}) &= \\ &\int_{-\infty}^{\infty} [G_{\sqrt{k_1^2+i\delta}}(\mathbf{x}; t, d)\tau_\delta^+(t) + \partial_{y_2} G_{\sqrt{k_1^2+i\delta}}(\mathbf{x}; t, d)\sigma_\delta^+(t)] dt + \\ &\int_{-\infty}^{\infty} [G_{\sqrt{k_1^2+i\delta}}(\mathbf{x}; t, -d)\tau_\delta^-(t) - \partial_{y_2} G_{\sqrt{k_1^2+i\delta}}(\mathbf{x}; t, -d)\sigma_\delta^-(t)] dt, \text{ for } |x_2| < d. \end{aligned} \tag{3.3}$$

For  $\delta > 0$  it is easy to see that the densities  $\{\sigma_\delta^\pm, \tau_\delta^\pm\}$  are decaying and have well behaved Fourier transforms. The densities also depend on  $\mathbf{y}$ , but to simplify the notation, we omit this argument.

Using the Sommerfeld formula we can re-express  $e_\delta(\mathbf{x}; \mathbf{y})$  in terms of the Fourier transforms of the densities,  $\{\hat{\sigma}_\delta^\pm, \hat{\tau}_\delta^\pm\}$ . For example, if  $x_2 > 0$ , then we have

$$e_\delta(\mathbf{x}; \mathbf{y}) = \frac{i}{4\pi} \int_{-\infty}^{\infty} \frac{e^{i(x_2-d)\sqrt{k^2+i\delta-\xi^2}} e^{ix_1\xi} [\hat{\tau}_\delta^+(\xi) + i\sqrt{k^2+i\delta-\xi^2}\hat{\sigma}_\delta^+(\xi)] d\xi}{\sqrt{k^2+i\delta-\xi^2}}. \tag{3.4}$$

Using these representations for  $e_\delta(\mathbf{x}; \mathbf{y})$  and  $\partial_{x_2} e_\delta(\mathbf{x}; \mathbf{y})$  where  $x_2 = \pm d$ , with  $f(\pm d^\pm) = \lim_{x \rightarrow \pm d^\pm} f(x)$ , the transmission boundary conditions are:

$$\begin{aligned} e_\delta(x_1, d^+; \mathbf{y}) + G_k(x_1, d; \mathbf{y}) &= e_\delta(x_1, d^-; \mathbf{y}), \\ e_\delta(x_1, -d^+; \mathbf{y}) &= e_\delta(x_1, -d^-; \mathbf{y}), \\ \partial_{x_2} e_\delta(x_1, d^+; \mathbf{y}) + \partial_{x_2} G_k(x_1, d; \mathbf{y}) &= \partial_{x_2} e_\delta(x_1, d^-; \mathbf{y}), \\ \partial_{x_2} e_\delta(x_1, -d^+; \mathbf{y}) &= \partial_{x_2} e_\delta(x_1, -d^-; \mathbf{y}). \end{aligned} \tag{3.5}$$

In the Fourier representation these take the form of a family of  $4 \times 4$  linear systems:

$$A_\delta(\xi) \mathbf{v}_\delta(\xi) = \mathbf{d}_\delta(\xi), \text{ for } \xi \in \mathbb{R}. \tag{3.6}$$

Here  $\mathbf{v}_\delta(\xi) = (\hat{\sigma}_\delta^+(\xi), \hat{\tau}_\delta^+(\xi), \hat{\sigma}_\delta^-(\xi), \hat{\tau}_\delta^-(\xi))^t$ , and  $\mathbf{d}_\delta(\xi)$  is obtained from the Sommerfeld representation of the data  $G_{\sqrt{k_1^2+i\delta}}(\mathbf{x}; \mathbf{y})$ . It is well known that these

matrices are invertible for  $\delta > 0$ . Let  $A_0(\xi) = \lim_{\delta \rightarrow 0^+} A_\delta(\xi)$ ; this matrix is invertible except for frequencies  $\{\xi_n\}$  for which

$$(\partial_{x_2}^2 + k^2(x_2) - \xi_n^2)v_n(x_2) = 0 \quad (3.7)$$

has an  $L^2$ -solution. There are finitely many such frequencies, which lie in  $[k, k_1]$ ; these correspond to *wave-guide modes* for the bi-infinite wave-guide, which are discussed in Section 2.1.

In fact the  $\det A_0(\xi)$  has simple poles at  $\{\pm\xi_n\}$ , which complicates the evaluation of  $\lim_{\delta \rightarrow 0^+} \mathbf{v}_\delta(\xi) = \lim_{\delta \rightarrow 0^+} A_\delta^{-1}(\xi)\mathfrak{D}_\delta(\xi)$ . The simplest thing to do is to assume that  $A_0(k) \neq 0$  and deform the contour of integration in (3.4), e.g. to a contour that replaces intervals around  $\{\pm\xi_n\}$  with semicircles centered on these points in either the upper or lower half planes, and then let  $\delta \rightarrow 0^+$ . Using the semi-circles in the upper half plane produces right-ward moving wave-guide modes, and those in the lower half plane, left-ward moving wave-guide modes. This is essentially the construction used in [16]. Since the poles of  $\det A_0(\xi)$  are simple, the limiting singularity of  $A_0^{-1}(\xi)$  takes the form

$$\lim_{\delta \rightarrow 0^+} \frac{a_n}{\xi - \xi_n + i\delta} = a_n \left[ \text{P. V.} \frac{1}{\xi - \xi_n} - i\pi\delta(\xi - \xi_n) \right],$$

as tempered distributions, which gives an alternate way to analyze the limiting densities, which are themselves tempered distributions.

### 3.1 Integral equation formulation

To solve (3.1), we first write it in a more generic form. We let  $\gamma$  be the union of the lines  $x_2 = \pm d$ , which are the discontinuities of  $q$ . We shall also let  $\mathbf{n}$  be the unit normal to  $\gamma$ , defined to point away from the region with wavenumber  $k_1$ . We will look for the solution  $v$  of

$$\begin{cases} (\Delta + k^2 + q(x_2))v = 0 & \text{in } \mathbb{R}^2 \setminus \gamma \\ [[v]]_\gamma = -[[v^{\text{inc}}]]_\gamma, & [[\partial_{\mathbf{n}}v]]_\gamma = -[[\partial_{\mathbf{n}}v^{\text{inc}}]]_\gamma \end{cases}, \quad (3.8)$$

plus appropriate radiation conditions. Clearly (3.1) is of this form with a particular choice of  $v^{\text{inc}}$ .

In order to numerically solve (3.8) we convert it into an integral equation supported on  $\gamma$ . To this end, we introduce the single and double layer potentials

$$\mathcal{S}_k[\rho](\mathbf{x}) = \int_\gamma G_k(\mathbf{x}; \mathbf{y})\rho(\mathbf{y})d\mathbf{y} \quad \text{and} \quad \mathcal{D}_k[\mu](\mathbf{x}) = \int_\gamma \partial_{\mathbf{n}_y}G_k(\mathbf{x}; \mathbf{y})\mu(\mathbf{y})d\mathbf{y}. \quad (3.9)$$

The operators  $\mathcal{S}_{k_1}$  and  $\mathcal{D}_{k_1}$  are defined similarly. As these layer potentials are integrals over unbounded domains and the kernels decay quite slowly, a rigorous study of these operators would require careful consideration to ensure that the integrals exist. In this paper however, we proceed formally, and assume that the integrals make sense.



Under this assumption, the function

$$v(\mathbf{x}) = \begin{cases} \mathcal{D}_k[\mu](\mathbf{x}) + \mathcal{S}_k[\rho](\mathbf{x}) & \text{if } |x_2| > d \\ \mathcal{D}_{k_1}[\mu](\mathbf{x}) + \mathcal{S}_{k_1}[\rho](\mathbf{x}) & \text{if } |x_2| < d \end{cases} \quad (3.10)$$

automatically satisfies the PDE in (3.8). We are therefore free to choose  $\rho$  and  $\mu$  so that  $v$  satisfies the transmission condition.

To enforce the transmission conditions, we introduce the normal derivatives of the layer potentials:

$$\mathcal{S}'_k[\rho](\mathbf{x}) = \int_{\gamma} \partial_{\mathbf{n}_x} G_k(\mathbf{x}; \mathbf{y}) \rho(\mathbf{y}) d\mathbf{y} \quad \text{and} \quad \mathcal{D}'_k[\mu](\mathbf{x}) = \int_{\gamma} \partial_{\mathbf{n}_x} \partial_{\mathbf{n}_y} G_k(\mathbf{x}; \mathbf{y}) \mu(\mathbf{y}) d\mathbf{y}, \quad (3.11)$$

where the  $\mathcal{D}'_k$  operator is interpreted in the Hadamard finite parts sense (see [28]).

If we use the well known jump relations for the single and double layer potentials (see [28]), then we find that  $v$  given by (3.10) satisfies the continuity conditions in (3.8) if

$$\left( \text{Id} + \begin{pmatrix} \mathcal{D}_k - \mathcal{D}_{k_1} & \mathcal{S}_k - \mathcal{S}_{k_1} \\ -(\mathcal{D}'_k - \mathcal{D}'_{k_1}) & -(\mathcal{S}'_k - \mathcal{S}'_{k_1}) \end{pmatrix} \right) \begin{pmatrix} \mu \\ \rho \end{pmatrix} = \begin{pmatrix} -[[v^{\text{inc}}]]_{\gamma} \\ [[\partial_{\mathbf{n}} v^{\text{inc}}]]_{\gamma} \end{pmatrix} \quad \text{on } \gamma. \quad (3.12)$$

We thus have that if  $\rho$  and  $\mu$  satisfy (3.12), then  $v$  defined by (3.10) solves (3.8).

Due to the presence of wave-guide modes, the solutions  $\rho$  and  $\mu$  do not decay as  $x_1 \rightarrow \pm\infty$ . Therefore the integral equation (3.12) cannot be numerically truncated at any value of  $x_1$ . We therefore use the coordinate complexification method introduced in the introduction. This is quite similar to the approach taken in [7].

In this method, we deform the boundary  $\gamma$  to the curve

$$\tilde{\gamma} = \{(x_1 + i\psi(x_1), \pm d) \mid x_1 \in \mathbb{R}\}, \quad (3.13)$$

where  $\psi$  is a monotonically increasing function supported on  $[-L, L]^C$ , which goes to  $\pm\infty$  as  $x_1 \rightarrow \pm\infty$ . The choice of  $L$  determines the strip of  $\mathbb{R}^2$  on which we can recover the solution  $u$ . We choose the normal to  $\tilde{\gamma}$  to be  $\mathbf{n} = (0, \text{sign}(x_2))$ , which agrees with the normal to  $\gamma$  where they overlap.

The integral operators on  $\tilde{\gamma}$  are the same as those on  $\gamma$ , except that they are based on the analytic continuation of the Green's function:

$$\tilde{G}_k(\mathbf{x}; \mathbf{y}) := \frac{i}{4} H_0^{(1)}(kr(\mathbf{x}; \mathbf{y})), \quad (3.14)$$

where

$$r(\mathbf{x}; \mathbf{y}) := \sqrt{(x_1 - y_1)^2 + (x_2 - y_2)^2}. \quad (3.15)$$

Choosing  $\psi$  to be non-decreasing ensures that

$$\Im[(x_1 - y_1 + i(\psi(x_1) - \psi(y_1)))^2 + (x_2 - y_2)^2] \geq 0, \quad (3.16)$$

for all  $x_1, y_1, x_2, y_2 \in \mathbb{R}$ . Therefore  $r(\cdot; \mathbf{y})|_{\tilde{\gamma}}$  does not cross the branch cut of the square root.

The advantage of this contour deformation comes from the fact that our kernels and densities are asymptotic to linear combinations of functions of the form

$$e^{i\eta\sqrt{x_1^2}(x_1^2)^{\alpha/2}} \quad (3.17)$$

for various choices of  $\eta$  and  $\alpha$ . When functions of this form are analytically continued to  $\tilde{\gamma}$ , they are bounded by the exponentially decaying functions

$$Ce^{-\eta|\Im x_1||x_1|^\alpha}. \quad (3.18)$$

This exponential decay allows us to truncate  $\tilde{\gamma}$  when  $|\Im x_1|$  is large enough.

## 3.2 Discretization

We now discuss a numerical method for solving the integral equation (3.12) on the contour  $\tilde{\gamma}$ . For the remainder of this paper, we take the complexification function to be defined by  $\psi(x_1) = 20 \operatorname{erfc}((x_1 + L + 30)/5) - \operatorname{erfc}(-(x_1 - L - 30)/5)$ , which is smooth and zero to machine precision on  $[-L, L]$ .

Since the densities decay exponentially on the non-real portions of  $\tilde{\gamma}$ , we can safely truncate without a great loss of accuracy. Specifically, since the slowest oscillation occurs at wavenumber  $k$ , there exists a constant  $C > 0$  such that

$$|\rho|, |\mu| < Ce^{-k|\Im x_1|}. \quad (3.19)$$

The estimate in (3.18) implies that we may truncate the contour when  $|\psi(x_1)|k > \log \epsilon$ , where  $\epsilon$  is a desired accuracy. In our experiments  $k$  is  $\sim 1$  and we choose the truncation  $\epsilon$  to be  $10^{-17}$ , so we can truncate at  $\Re x_1 = \pm(L + 38)$ .

On this truncated contour, the integral equation can be discretized using standard techniques. Specifically, we solve it using the chunkIE package [3], which solves integral equations using a modified Nyström discretization. The contour  $\tilde{\gamma}$  is split into panels  $\gamma_i$ , each of which is represented by 16th order Gauss-Legendre nodes. Overall, the contour is represented by nodes  $\mathbf{x}_1, \dots, \mathbf{x}_{n_{\text{chunk}}}$ . The unknowns  $\rho$  and  $\mu$  are represented by their values at the  $\mathbf{x}_i$ 's, which we denote by  $\rho_i$  and  $\mu_i$ .

To evaluate integral operators at a target  $\mathbf{x}$ , we do integrals one panel at a time. If the target is far from the panel  $\gamma_i$ , then we use the Gauss-Legendre quadrature rule, which is well suited to the smooth quadratures. When  $\mathbf{x}$  is near but not on  $\gamma_i$ , we use adaptive integration to integrate the interpolant of  $\rho$  and  $\mu$ . When  $\mathbf{x}$  is in  $\gamma_i$ , we use generalized Gaussian quadrature [10]. With the above quadrature rules, we can build a discrete linear system that enforces (3.12) at each node  $\mathbf{x}_i$ .

We solve this discretized equation using the recursive skeletonization algorithm implemented in the *Fast Linear Algebra in MATLAB* (FLAM) software library [22]. This algorithm builds a fast direct solver for (3.12), which is particularly appropriate for this problem because we must solve the equation with a

different right hand side every time we wish to evaluate  $G_q$ . The cost of building this fast direct solver is  $O(n^2)$ , and once it has been built the cost of each solve is  $O(n)$ . Once we have solved (3.12), the solution  $u$  can be recovered through the representation (3.10) and the previously discussed quadrature rules.

### 3.3 Numerical verification

We test our solver with  $k = 1, k_1 = 2$ , and  $d = 2$ , and begin with an analytic solution test by picking the incoming field  $v^{\text{inc}}$  such that the true solution is known. Specifically, if we let  $\mathbf{x}_0 = (0, 1)$ , then it is not hard to see that

$$v^{\text{inc}}(\mathbf{x}) = \begin{cases} \tilde{G}_k(\mathbf{x}; \mathbf{x}_0) & \text{if } |x_2| > d \\ 0 & \text{if } |x_2| < d \end{cases}. \quad (3.20)$$

solves (3.8) with  $v = v^{\text{inc}}$ . We may therefore numerically solve (3.8) using the method described in this section and compare the numerical solution to the true solution (3.20). In Figure 3, we show the accuracy when  $\tilde{\gamma}$  is discretized using 72 16th-order panels and  $L = 10$ . The maximum error is determined by the adaptive integration tolerance, which is  $10^{-12}$ .

To check that the solver does not depend on  $L$  and our truncation distance, we redo the experiment with those distances and the number of points doubled. In this test, the maximum error is still comparable to the adaptive integration tolerance. We also redo the experiments with  $\tilde{\gamma}$  truncated at  $|\Re x_1| = L + 25$ . This time the maximum error is  $1.3 \times 10^{-7}$  because we did not go far enough out into the complex plane to ensure that the densities had sufficiently decayed. This can easily be seen from the graph of the corresponding densities are shown in Figure 4.

Now that we have completed the construction of our solver, we are able to evaluate  $G_q$  and it's derivatives. A few examples are shown in Figure 5.

## 4 Solving the matched IE

In this section, we discuss the numerical solution of (2.14). In order to truncate the problem, we again use coordinate complexification. In particular, we solve (2.14) on the deformed contour

$$\hat{\gamma} = \{(0, y_2 + i\psi(y_2)); 0, x_2 + i\psi(x_2)\} | y_2, x_2 \in \mathbb{R}\}. \quad (4.1)$$

We defer the proof that (2.14) is well posed on  $\hat{\gamma}$  to a future paper. Here we simply observe that the wave-guide Green's function,  $G_{q_i, r}$ , can be analytically continued to  $\hat{\gamma}$ , and so (2.14) can at least be defined. This follows from the Fourier representation of  $G_{q_i, r}$  given in [16]. For the sake of brevity, we defer a rigorous justification to [46].

We discretize (2.14) on  $\hat{\gamma}$  in the same way we discretized (3.12) in Section 3.2, except that the integral operators are built using the wave-guide Green's functions. We let  $\mathbf{z}_i$  be the nodes used to discretize  $\hat{\gamma}$  and assume that there are  $m$  of them.

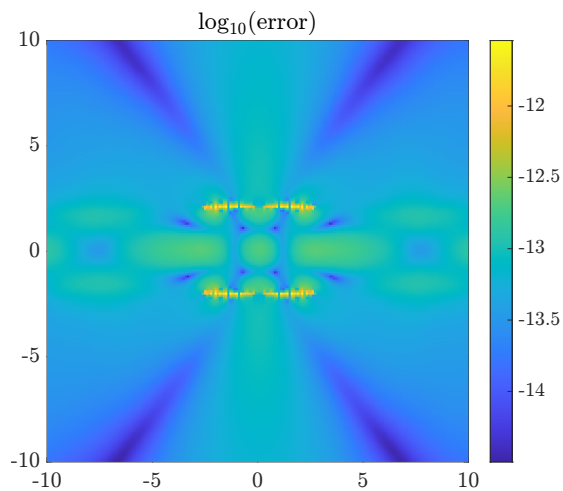


Figure 3: The analytic solution test for our single wave-guide solver. We see that the solver is accurate to at least the adaptive integration tolerance  $10^{-12}$  everywhere.

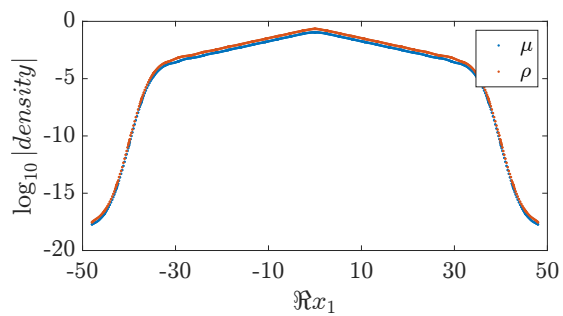


Figure 4: The modulus of the solution densities from the analytic solution test in Figure 3. The densities from the two halves of  $\tilde{\gamma}$  overlap because of the symmetry of the problem and solution. The figure clearly shows that contour deformation was enough to ensure that the densities have decayed to machine precision.

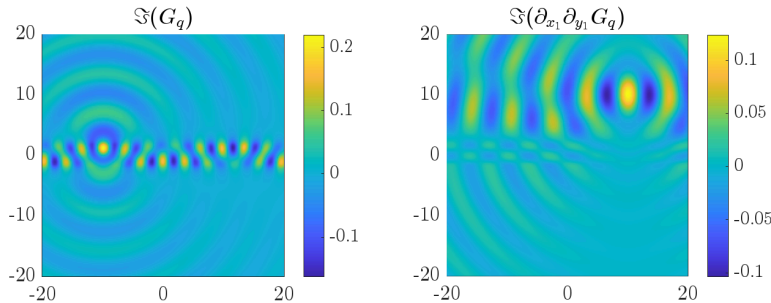


Figure 5: An example of  $G_q$  and one of its derivatives.

At this point, we have all the tools needed to accurately solve (2.14). However, a solver based on this discretization would be slow, as each evaluation of  $G_{q_l, r}$  requires us to solve (3.12). The two halves of the problem, building the system matrix and recovering the solution, require different approaches to handle this slowness. In the remainder of this section, we explain how those computations can be accelerated, starting with reconstruction of the solution.

Once we have solved for  $\sigma$  and  $\tau$ , the naive evaluation of the field  $u_l = \mathcal{S}_{q_l}[\tau] + \mathcal{D}_{q_l}[\sigma]$  at each target costs  $O(nm)$ . If there  $n_t$  targets, then the cost becomes  $O(n_t nm)$ , which is infeasibly large. To accelerate this computation, we note that  $u_l(\mathbf{x})$  is a solution of (3.8) with

$$v^{\text{inc}}(\mathbf{x}) = \sum_i G_{k_l, r}(\mathbf{x}; \mathbf{z}_i) \tau_i w_i + \partial_{z_1} G_{k_l, r}(\mathbf{x}; \mathbf{z}_i) \sigma_i w_i. \quad (4.2)$$

Evaluating the right hand side of (3.12) with this incoming field costs  $O(nm)$ . Solving (3.12) then costs  $O(n)$  and evaluating (3.10) costs  $O(n_t n)$ . If we add the cost of evaluating  $v^{\text{inc}}$  at all the targets,  $O(n_t m)$ , then we can see that the total cost to evaluate  $u_l$  can be brought from  $O(n_t nm)$  down to  $O(n_t(n + m) + nm)$ . This lower cost makes it possible to create high resolution plots of the solution. If desired, one could accelerate this to linear complexity using an FMM [47]. A nice feature of this approach, is that it is completely general. We can therefore use it for any decomposable problem.

We now turn to solving (2.14). The simplest approach would be to avoid building the system matrix entirely, and solve (2.14) using an iterative solver. We could then use the strategy described above to apply most of the system matrix quickly. The singular quadrature for close sources and targets would have to be handled separately, which would greatly slow down the algorithm.

Instead, we build a compressed representation of the wave-guide Green's function. For  $\mathbf{z}_i$  far from the wave-guides, this representation is built using low rank factorizations. When those are not available, we use Chebyshev expansions. In the remainder of this section we spell out these steps in more detail. To keep things simple, we build separate compressions for  $G_{q_l}^{\text{out}}$  and  $G_{q_r}^{\text{out}}$  and suppress

the dependence on  $l, r$  in our discussion.

## 4.1 Outgoing skeleton

When building the system matrix, we must compute

$$v(\mathbf{z}_i) = \mathcal{S}_k[\rho] + \mathcal{D}_k[\mu] \approx \sum_{j=1}^n G_k(\mathbf{z}_i; \mathbf{x}_j) w_j \rho_j + \partial_{\nu_j} G_k(\mathbf{z}_i; \mathbf{x}_j) w_j \mu_j \quad (4.3)$$

for every  $i$  and with a different pair of densities for each source. We therefore desire a way to evaluate this sum quickly.

We let  $E$  be the matrix mapping from  $\rho_j$  and  $\mu_j$  to  $v(\mathbf{z}_i)$ . Let  $Z_F = \{\mathbf{z}_i\}_{i \in I_F}$  be the set of  $\mathbf{z}_i$ 's that are at least a wavelength from any of the  $\mathbf{x}_j$  and  $E_F = E(I_F, \cdot)$ . The submatrix  $E_F$  is numerically low rank provided the extent of  $\mathbf{x}_j$ 's and  $\mathbf{z}_i$ 's is not too large (see [47]). We can therefore apply a large slice of  $E$  using a low rank factorization of  $E_F$ .

A particularly nice factorization, is the interpolative decomposition

$$E_F \approx E_F(:, J_{\text{out-skel}}) T, \quad (4.4)$$

where  $J_{\text{out-skel}}$  represents an ‘‘important’’ set of sources and  $T$  is an interpolation matrix. We refer to  $J_{\text{out-skel}}$  as the *outgoing skeleton* of  $\tilde{\gamma}$ . Physically, the factorization (4.4) is equivalent to the statement

$$v(\mathbf{z}_i) \approx \sum_{j \in J_{\text{out-skel}}} \mathcal{G}_j(\mathbf{z}_i; \mathbf{x}_j) \left[ T \begin{pmatrix} \rho \\ \mu \end{pmatrix} \right]_j, \quad (4.5)$$

for  $i \in I_F$ , where  $\mathcal{G}_j$  is  $G_k$  or  $\partial_{\mathbf{n}_j} G_k$ .

In practice, this idea has a few drawbacks. Namely that we must build a different factorization for  $\partial_{z_2} v$  and if we change  $\tilde{\gamma}$ . It is therefore advantageous to design  $J_{\text{out-skel}}$  and  $T$  such that (4.5) holds for a more flexible choice of  $\mathbf{z}$ 's. A common strategy when all the points are in  $\mathbb{R}^2$  is to ensure that (4.5) holds for all  $\mathbf{z}$  on a curve  $\gamma_P$ , called a proxy curve, that encompasses the points in  $Z_F$  (see [30]). A fairly simple argument using Green's identity shows that if (4.5) holds on  $\gamma_P$ , then it holds for every point inside  $\gamma_P$  and also for the derivatives of  $v$ . We shall use this idea to build our factorization, with  $\gamma_P$  being a curve that encompasses the real parts of the points in  $Z_F$  and is at least a wavelength from any  $\mathbf{x}_j$ .

The proof that a skeleton built using this  $\gamma_P$  gives correct answers for complex  $\mathbf{x}$  and  $\mathbf{z}$  is the subject of ongoing work. We therefore present numerical evidence that the proxy curve is applicable to this case. We choose  $\gamma_P$  to be the union of boundaries of the boxes

$$B_+ = [-1, 1] \times [d + 2\pi/k, 100] \text{ and } B_- = [-1, 1] \times [-100, -d - 2\pi/k].$$

We build the outgoing skeleton such that (4.5) holds to a tolerance  $\epsilon$  for 300 points on each segment of  $\gamma_P$ .

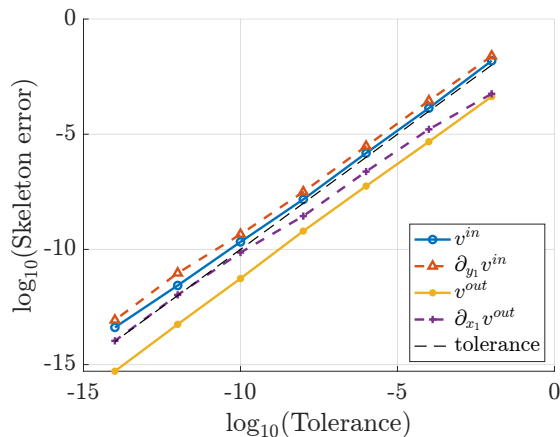


Figure 6: The error in the formulas (4.5) and (4.9) as a function of the tolerance used to build the skeletons. The error presented is a maximum over points spread out in the boxes  $B_{\pm}$ .

We then test the skeletonization error, i.e. the error in (4.5), on a grid of 250 targets in each  $B_{\pm}$ . Figure 6 shows how the maximum interpolation error depends on the tolerance used to build the skeleton. As we can see, the interpolation error matches the tolerance, and so the proxy curve can be used with complex  $\mathbf{x}_j$ . Similar results are found when we take the  $x_1$ -derivative of (4.5), which will be required to evaluate  $\partial_{x_1} v$ . We also added imaginary parts  $\Im z_2 = \psi(\Re z_2)$  to the targets and found identical results.

By refining  $\tilde{\gamma}$ , we also observed the the number of skeleton points is independent (within  $\pm 1$ ) of the number of panels in  $\tilde{\gamma}$ .

## 4.2 Incoming skeletons

Building the system matrix also requires us to evaluate many different right hand sides for (3.12). Namely, we must evaluate

$$f_{ij} := G_k(\mathbf{x}_i; \mathbf{z}_j) - G_{k_1}(\mathbf{x}_i; \mathbf{z}_j) \quad (4.6)$$

and

$$g_{ij} := \partial_{n_i} G_k(\mathbf{x}_i; \mathbf{z}_j) - \partial_{n_i} G_{k_1}(\mathbf{x}_i; \mathbf{z}_j) \quad (4.7)$$

for every  $i$  and  $j$ . We denote the combined matrix of  $f_{ij}$  and  $g_{ij}$ 's by  $R$ . The slice of  $R$  corresponding to  $\mathbf{z}_j \in Z_F$  is  $R_F$ . This slice has a low rank factorization for the same reason as  $E_F$  does. We shall therefore work to build its interpolative decompositions

$$R_F \approx X R(I_{\text{in-skel}}, :). \quad (4.8)$$

We refer to  $I_{\text{in-skel}}$  as the *incoming skeleton* of  $\tilde{\gamma}$ . Since  $G_k - G_{k_1}$  does not satisfy a Green's theorem, we can not directly use a proxy curve to build this

factorization. Instead, we therefore build a skeleton that works for each kernel separately, i.e. we choose  $I_{\text{in-skel}}$  and  $X$  such that

$$G_{\tilde{k}}(\mathbf{x}_i; \mathbf{z}_j) \approx \sum_{l \in I_{\text{in-skel}}} X_{il} \tilde{\mathcal{G}}_l(\mathbf{x}_l; \mathbf{z}_j) \quad (4.9)$$

and

$$\partial_{\mathbf{n}_i} G_{\tilde{k}}(\mathbf{x}_i; \mathbf{z}_j) \approx \sum_{l \in I_{\text{in-skel}}} X_{(i+n)l} \tilde{\mathcal{G}}_l(\mathbf{x}_l; \mathbf{z}_j), \quad (4.10)$$

where  $\tilde{\mathcal{G}}_l = G_{\tilde{k}}$  or  $\partial_{\mathbf{n}_i} G_{\tilde{k}}$  and  $\tilde{k} = k, k_1$ . Since  $G_k$  and  $G_{k_1}$  independently satisfy Green's identities, we can build this factorization using the same proxy curve  $\gamma_P$  as we used to build the outgoing skeleton.

**Remark 1.** *The incoming skeleton described here could be used an outgoing skeleton. In practice, we chose not to reuse the skeletons to keep the outgoing skeleton as small as possible.*

We test our incoming skeleton, in the same way as the outgoing section in the previous section. Figure 6 shows that the skeletonization error matches the tolerance used to compare the skeleton, as we would hope. Finally, we observe that the same skeleton can be used to compute  $\partial_{y_1} G_q^{\text{out}}$ .

### 4.3 Far sources and far targets

In this section, we show how the incoming and outgoing skeletons can be used to build a fast evaluator for  $G_q^{\text{out}}(\mathbf{x}; \mathbf{y})$  when  $\mathbf{x}, \mathbf{y} \in Z_f$ . As described in the previous section, for any source  $\mathbf{y}$  in  $B$ , we can efficiently evaluate the right hand side of (2.14) by applying  $X$  to the vector

$$\text{rhs}_j(\mathbf{y}) = [[\tilde{\mathcal{G}}_j(\mathbf{x}_j; \mathbf{y})]]_{\tilde{\gamma}}. \quad (4.11)$$

We can therefore compute the densities as

$$(\mu(\mathbf{z}); \rho(\mathbf{y})) = K^{-1} X \text{rhs}(\mathbf{y}), \quad (4.12)$$

where  $K$  is the system matrix for (3.12). This formula is helpful because  $K^{-1}X$  can be precomputed allowing us to efficiently solve (3.12) for any source  $\mathbf{y} \in Z_f$ . We can efficiently evaluate the potentials generated by these densities using (4.5). Putting it all together we have the formula

$$G_q^{\text{out}}(\mathbf{x}; \mathbf{y}) \approx \sum_{j \in J_{\text{out-skel}}} \mathcal{G}_j(\mathbf{x}; \mathbf{x}_j) [(TK^{-1}X) \text{rhs}(\mathbf{y})]_j, \quad (4.13)$$

which is accurate for any  $\mathbf{x}, \mathbf{y} \in Z_F$ . If we precompute  $TK^{-1}X$ , then this formula can be used to evaluate  $G_q^{\text{out}}$  in  $O(n_{\text{in-skel}}n_{\text{out-skel}})$  time, independent of the number of points in  $\tilde{\gamma}$ .

We test this approach by finding the error in computing  $G_q^{\text{out}}(\mathbf{x}; \mathbf{y})$  for every pair of points used in Section 4.1. Figure 7 shows how the maximum of these



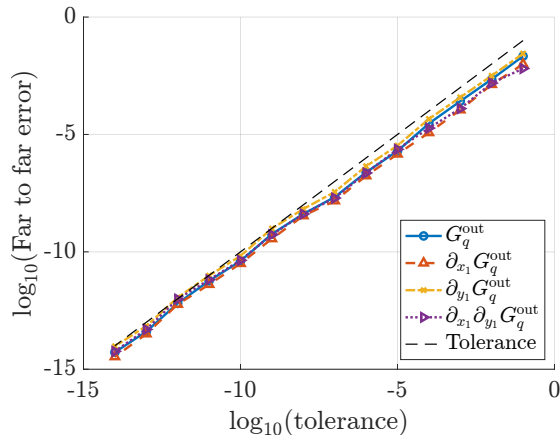


Figure 7: This figure shows how the error when (4.13) is used to approximate  $G_q^{\text{out}}(\mathbf{x}; \mathbf{y})$  and its derivatives depends on the skeletonization tolerance. The error reported is the maximum pointwise error over points spread out in the boxes  $B_{\pm}$ .

errors scales with the tolerance used to compute the skeletons. To further test this method, we check the error in the equivalent formulas for  $\partial_{x_1} G_q^{\text{out}}$ ,  $\partial_{y_1} G_q^{\text{out}}$ , and  $\partial_{x_1} \partial_{y_1} G_q^{\text{out}}$ . We can see that all of the errors scale with the skeletonization tolerance correctly.

#### 4.4 Far sources and near targets

When the target  $\mathbf{x}$  is not in  $Z_F$ , we are not able to use the outgoing skeleton to compute  $G_q^{\text{out}}(\mathbf{x}; \mathbf{y})$ . We therefore need a different way to quickly evaluate  $G_q^{\text{out}}$ . When  $\mathbf{y} \in Z_F$ , (4.12) tells us that  $G_q^{\text{out}}(\mathbf{x}; \mathbf{y})$  can be written as a linear combination of the potentials generated by the densities that are the columns of  $K^{-1}X$ . It therefore remains to find an efficient way to generate those potentials.

Let  $v_i$  be the field generated by the  $i$ th column of  $K^{-1}X$ . In order to rapidly evaluate those fields, we shall generate piecewise Chebyshev interpolants of  $u_i(0, \cdot)$ . Let  $I_1, \dots, I_N$  be a collection of intervals that partition the interval  $[-d - 2\pi/k, d + 2\pi/k]$  such that  $q$  is constant on each interval. Typically, we shall use one interval per region that  $q$  is constant, but wide or high frequency wave-guides may need more intervals.

On each of the intervals  $I_1, \dots, I_N$  we build a Chebyshev expansion. If  $l_j$  and  $c_j$  are length and center of  $I_j$ , then this takes the form.

$$v_i(0, x_2) \approx \sum_{l=1}^p a_{i,l,j} T_l \left( 2 \frac{x_2 - c_j}{l_j} \right) \quad \forall x_2 \in I_j. \quad (4.14)$$

In general, we have no guarantee that the  $v_i$ 's are nice functions in the neighbourhood of  $\tilde{\gamma}$ . We therefore do not expect  $v_i(0, \cdot)$  to be smooth so these

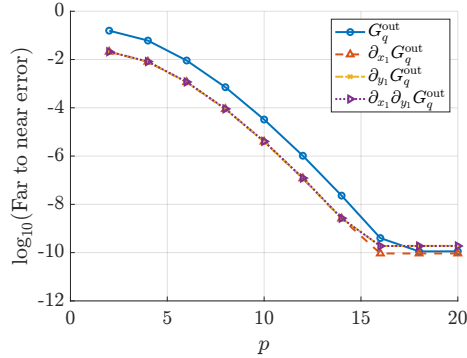


Figure 8: This figure shows how the error in (4.14) depends on the order of the Chebyshev expansions.

Chebyshev expansions may not converge. Fortunately, we do not need to evaluate individual  $v_i$ 's. Instead we only use linear combinations of the  $v_i$ 's. Indeed (4.12) is equivalent to the statement that

$$G_q^{\text{out}}(0, x_2; \mathbf{y}) \approx \sum_{i \in I_{\text{in-skel}}} v_i(0, x_2) \mathcal{G}_i(\mathbf{x}_i; \mathbf{y}) \quad (4.15)$$

for all  $x_2 \in \hat{\gamma}$ . If we plug our expansions of  $v_i$  into this expression, then we find

$$G_q^{\text{out}}(0, x_2; \mathbf{y}) \approx \sum_{l=1}^p \left( \sum_{i \in I_{\text{in-skel}}} a_{i,l,j} \mathcal{G}_i(\mathbf{x}_i; \mathbf{y}) \right) T_l \left( 2 \frac{x_2 - c_j}{l_j} \right) \quad (4.16)$$

for all  $x_2 \in I_j$ . Equation (4.16) is a Chebyshev interpolant of  $G_q^{\text{out}}(0, x_2; \mathbf{y})$ , up to the tolerance used in the skeletonization and solving (3.12). Since  $\mathbf{y} \in Z_F$ , the function  $G_q^{\text{out}}(0, x_2; \mathbf{y})$  is a solution of (3.8) with smooth boundary data. The Chebyshev interpolant (4.16) therefore converges spectrally, making (4.16) an efficient and accurate method for computing  $G_q^{\text{out}}(0, x_2; \mathbf{y})$ .

To test this algorithm, we build the incoming skeletonization with a tolerance of  $10^{-10}$  and build the Chebyshev expansions (4.14) with various lengths  $p$ . We test the interpolation accuracy using the same grid of sources used to test the incoming skeleton and 100 targets evenly spaced on the line  $\{0\} \times (\cup_j I_j)$ . The maximum errors are reported in Figure 8. We can see that the errors do indeed converge spectrally with  $p$  up to the skeletonization tolerance.

Since some of our matrix entries need  $x_1$  derivatives of  $G_q$ , we also build Chebyshev expansions of  $\partial_{x_1} v_i(0, x_2)$ . We then test the equivalent formulas to (4.16) for all of the required derivatives of  $G_q^{\text{out}}$ . Figure 8 shows that these interpolants are also spectrally accurate.

In theory, the interpolation error can also be determined by the discretization error in (3.12). However, since  $\mathbf{y}$  is far from  $\hat{\gamma}$ , the densities are well resolved and adaptive integration is used to ensure that the  $v_i$ 's are computed accurately.

## 4.5 Near sources and far targets

We can use a similar idea to the previous section when  $\mathbf{x} \in Z_F$  but  $\mathbf{y}$  is not. By (4.5), for any  $\mathbf{x} \in Z_F$  we have that

$$G_q^{\text{out}}(\mathbf{x}; 0, y_2) \approx \sum_{i \in J_{\text{out-skel}}} \mathcal{G}_i(\mathbf{x}; \mathbf{x}_i) \left[ T \begin{pmatrix} \rho(0, y_2) \\ \mu(0, y_2) \end{pmatrix} \right]_i \quad (4.17)$$

We build piecewise Chebyshev expansions of the density skeletons on each subinterval:

$$\left[ T \begin{pmatrix} \rho(0, y_2) \\ \mu(0, y_2) \end{pmatrix} \right]_i = \sum_{l=1}^p b_{i,l,j} T_l \left( 2 \frac{y_2 - c_j}{l_j} \right) \quad \forall y_2 \in I_j. \quad (4.18)$$

Plugging these expansions into (4.17) gives

$$G_q^{\text{out}}(\mathbf{x}; 0, y_2) \approx \sum_{l=1}^p \left( \sum_{i \in J_{\text{out-skel}}} b_{i,l,j} \mathcal{G}_i(\mathbf{x}; \mathbf{x}_i) \right) T_l \left( 2 \frac{y_2 - c_j}{l_j} \right), \quad (4.19)$$

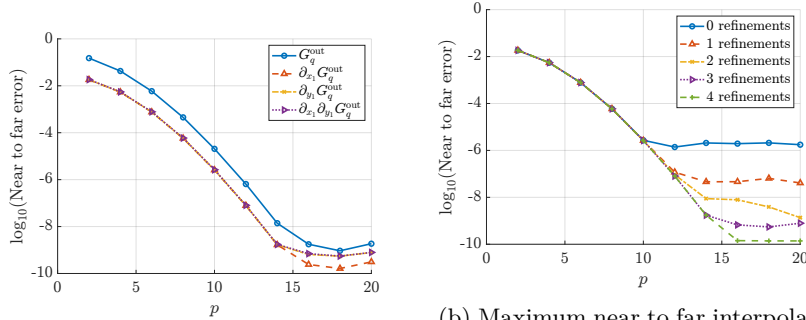
which is a Chebyshev expansion on the interval  $I_j$ . Since  $G_q^{\text{out}}(\mathbf{x}; 0, y_2)$  is a piecewise smooth function of  $y_2$ , this expansion converges spectrally up to the error in the skeletonization and the discretization of (3.12).

To test this algorithm, we build the outgoing skeletonization with a tolerance of  $\epsilon = 10^{-10}$  and build the Chebyshev expansions (4.18) with various lengths  $p$ . We compute the interpolation accuracy using the same grid of targets used to test the outgoing skeleton and 100 sources evenly spaced on the line  $\{0\} \times (\cup_j I_j)$ . The maximum errors are reported in Figure 9a. We can see that the errors do indeed converge super-algebraically with  $p$ .

We can use similar formulas to compute the derivatives  $G_q^{\text{out}}$ , except that new expansions must be build for the  $y_1$  derivative of the densities. We test the accuracy of these for all of the required derivatives of  $G_q^{\text{out}}$ . Figure 8 shows these interpolants also work as expected.

In all of these experiments, the error stagnates at a value higher than would caused by the skeletonization. This is due to the densities not being sufficiently resolved when the sources and Chebyshev nodes are quite close to  $\tilde{\gamma}$ . To verify this observation, we repeat the same experiment with several different discretizations of  $\tilde{\gamma}$  and the highest order required derivative of  $G_q^{\text{out}}$ . Figure 9b shows that the stagnation point does indeed depend on the discretization and can be pushed down to the skeletonization tolerance. When we solve (2.14) in Section 6, this experiment helps us to decide how much to refine  $\tilde{\gamma}$ .

**Remark 2.** *It is sometimes the case that we would like to know the solution a great distance from the waveguide. We can achieve this by iteratively extending the computational domain in a manner similar to that described in [23]. This is cheaper than solving directly, as it only requires us to evaluate the waveguide Green's functions at targets far from the waveguides. Due to the way we have constructed the skeletons, they can be reused in each iteration.*



(a) Maximum near to far interpolation error as a function of the order of the Chebyshev expansions for the various derivatives of  $G_q^{\text{out}}$

(b) Maximum near to far interpolation error as a function of the number of refinements of the boundary  $\tilde{\gamma}$ .

Figure 9: These figures shows how the error in (4.19) varies with the expansion order and the discretization of  $\tilde{\gamma}$ .

## 4.6 Near sources and near targets

We now turn to the final case. When neither  $\mathbf{x}$  nor  $\mathbf{y}$  are in  $Z_F$ , we cannot use skeletonization to build efficient evaluators. We therefore simply use tensor product Chebyshev expansions for each pair of subintervals  $I_i$  and  $I_j$ . We show below that there are more efficient compression schemes, but this is sufficient for our purposes. Since we only build these expansions for the region close to  $\tilde{\gamma}$ , we do not need too many subintervals and the precomputation is not too costly. It remains, however, to analyze their accuracy.

The accuracy is determined by the smoothness of  $G_q^{\text{out}}(0, x_2; 0, y_2)$ . The following lemma summarizes some results in [16].

**Lemma 1** ([16]). *The function  $G_q^{\text{out}}(0, x_2; 0, y_2)$  and its derivatives are smooth in each region where  $q$  is constant apart from a singularity as  $x_2, y_2 \rightarrow \pm d$ .*

*In that limit the derivatives of  $G_q^{\text{out}}$  satisfy*

$$\partial_{\mathbf{x}, \mathbf{y}}^\alpha G_q^{\text{out}}(0, x_2; 0, y_2) \sim (x_d + y_d)^{2-|\alpha|} \log(x_d + y_d), \quad (4.20)$$

where  $\alpha$  is a multi index of derivatives and

$$x_d = ||x_2| - d| \quad \text{and} \quad y_d = ||y_2| - d|. \quad (4.21)$$

The statement in Lemma 1 is slightly different than is given in [16] because we have chosen  $v^{\text{inc}} = G_{k(\mathbf{x})}$  rather than  $G_k$ .

To test our compressed representation, we place 100 equally spaced points on the line  $\{0\} \times [-d - 2\pi/k, d + 2\pi/k]$  and compute  $G_q^{\text{out}}(0, x_2; 0, y_2)$  for every pair of points. Due to the singularities indicated by Lemma 1, the Chebyshev expansions do not converge in an  $L^\infty$  sense. We therefore report an approximation of the  $L^2$ -error in Figure 10. We see that the error converges to expected

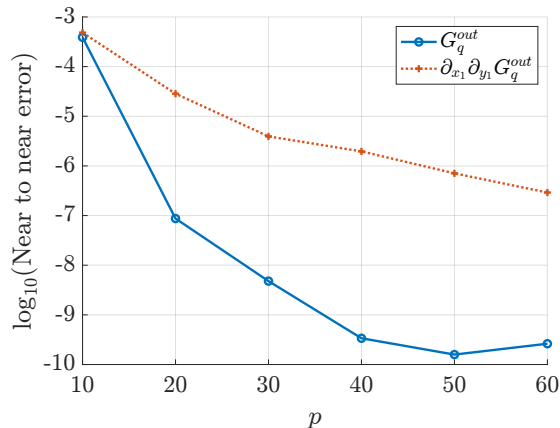


Figure 10: Our near to near test

value as we increase  $p$ , albeit slowly. We could obtain better convergence by building the singularities in Lemma 1 into our expansion. However, the errors shown in Figure 10 are small enough for our purposes.

## 5 Numerical experiments

We now test the numerical solver developed in the previous section. We choose  $k = 1$  and set  $k_{1;l} = 2, d_l = 2; k_{1;r} = 3, d_r = 4$  so that

$$q_l(x_2) = (2^2 - 1)\chi_{[-2,2]}(x_2) \quad \text{and} \quad q_r(x_2) = (3^2 - 1)\chi_{[-4,4]}(x_2). \quad (5.1)$$

We discretize  $\hat{\gamma}$  using 96 16th order panels and  $L = 10$ . We build the skeletonization with a tolerance of  $10^{-10}$  and build the expansions (4.14) and (4.18) to order 20. The other expansions are built to order 60.

We set

$$v_l^{\text{inc}}(\mathbf{x}) = -G_{q_l}(\mathbf{x}; \mathbf{x}_0), \quad (5.2)$$

where  $\mathbf{x}_0 = (-10, 0)$ , and  $v_r^{\text{inc}} = 0$ . Figure 11a shows the resulting total field. To test the accuracy of our solve, we re-solve this problem with twice as many points on the contour  $\hat{\gamma}$ . The error in this experiment is shown in Figure 12. As we can see, the error is quite small away from  $\hat{\gamma}$ . The solution is less accurate around  $\hat{\gamma}$  because the integrals in (2.11) become nearly singular, something that could be resolved using adaptive integration. We thus conclude that we have solved our problem to the accuracy allowed by our compression algorithms.

It is interesting to observe the behaviour of the densities  $\sigma$  and  $\mu$ . From Figure 11b, we can make two observations. The first is that the contour deformation has indeed caused the densities to exponentially decay and so we have truncated  $\hat{\gamma}$  in a reasonable location. The second observation is that the densities are smooth on each side of boundaries of the wave-guides. This is a nice

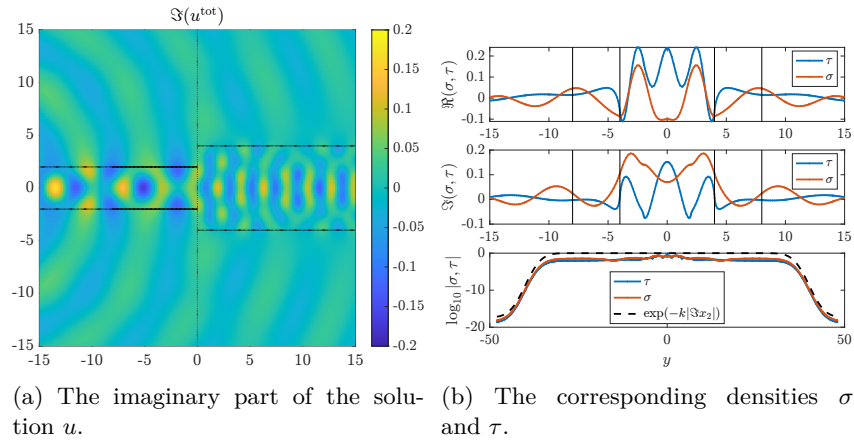


Figure 11: These figures show a solution of the matched wave-guide problem in the case where two wave-guides meet along the  $x_2$ -axis.

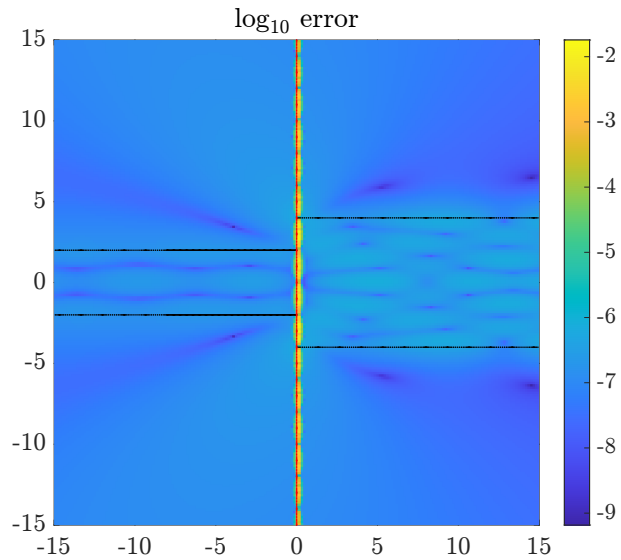


Figure 12: The estimated error in our self convergence study. We can see that the solution is accurate to 6 digits everywhere away from  $\hat{\gamma}$ .

feature of our integral equation. Even though the underlying PDE has a corner at those points, the integral equation is not singular there.

To further test our discretization, we use an analytic solution test similar to the one in Section 3.3. We redo the experiment with  $\mathbf{x}_0 = (10, 0)$ . In this case the solution of (1.2) is

$$u(\mathbf{x}) = \begin{cases} G_{q_l}(\mathbf{x}; \mathbf{x}_0) & \text{if } x_1 < 0 \\ 0 & \text{if } x_1 > 0. \end{cases} \quad (5.3)$$

The errors in the numerical solution are comparable to the self-convergence error estimate in Figure 12, except they are about digit better. We can thus conclude that we are indeed able to accurately solve (1.2). The increased accuracy is due the fact that the solution, in this, case does not have a singularity at the intersection of  $\tilde{\gamma}$  and  $\hat{\gamma}$ , whereas the solution in the previous test has weak singularities there.

To verify that the choice of  $L$  in  $\psi$  and our choice of truncation do not affect the accuracy, we redo the analytic solution test with  $L$ , the truncation distance, and the number of points doubled. There error is still bounded by  $10^{-6}$  and so we have chosen these parameters sufficiently large.

## 6 The scattering matrix and radiated power

In the design process, it is often important to know how much power is transferred through a junction, how much is reflected, and how much is lost to radiation. This information is encoded in the scattering matrix. With the ability to compute scattering matrices, we can build a very efficient simulation of an optical circuit. In this section, we describe how to build the scattering matrix and how to use it to measure the radiated power.

### 6.1 Finding the wave-guide modes

As described above, the wave-guide modes are of the form

$$u_{j;l,r,\pm}(x_1, x_2) = e^{\pm i\xi_{j;l,r} x_1} v_{j;l,r}(x_2). \quad (6.1)$$

where the  $v_{j;l,r}(x_2)$ 's are the solution of (2.2). The  $\xi_{j;l,r}$ 's are the roots of (2.3) that lie in the interior of  $(k, k_{1;l,r})$ . To find these roots, we use the smoother equivalent form of equation (2.3)

$$f_{l,r}(\xi) = (k_{1;l,r}^2 + k^2 - 2\xi^2) \sin\left(2d\sqrt{k_{1;l,r}^2 - \xi^2}\right) - 2\sqrt{\xi^2 - k^2} \sqrt{k_{1;l,r}^2 - \xi^2} \cos\left(2d\sqrt{k_{1;l,r}^2 - \xi^2}\right) = 0. \quad (6.2)$$

Not that while  $k_{1;l,r}$  is always a root of this equation it is never a root of the Wronskian.

To find the roots of  $f_{l,r}$ , we build a 500 term Chebyshev expansion of each function. To avoid a loss of accuracy caused by the square root singularities, we build this expansion on the interval  $(k + 0.01, k_{1;l,r} - 0.01)$ , which allows us to find all of the modes for most wave-guides. Wave-guides with modes outside this interval could be handled with a longer expansion over a bigger interval. We find the roots of those expansions using their colleague matrices (see [20]). Any roots of those expansions that lie in  $(k + 0.01, k_{1;l,r} - 0.01)$  are the frequencies of the wave-guide modes.

Now that we have found these modes, we can compute the projection of  $u$  onto them. The projection onto  $u_{j;r,+}$  is defined to be

$$c_j^r = \int_{-\infty}^{\infty} \overline{u_{j;r,+}(x_1, x_2)} u(x_1, x_2) dx_2 \quad (6.3)$$

for any  $x_1 > 0$ . The projections onto  $u_{j;l,-}$  are defined similarly. By equation (206) in [16], these coefficients can also be computed by the formula

$$c_j^r = \int_{-\infty}^{\infty} v_{r,j}(x_2) (-i\xi_j^r \sigma + \tau) dx_2. \quad (6.4)$$

As further verification of our solver, we compute the projections of  $u$  in Figure 11a using both formulas. We discretize (6.3) using  $x_1 = 5$  and  $x_1 = 25$  and eight 16th order Gauss-Legendre panels on the numerical support of the wave-guide modes. The the difference in each of the computed coefficients was less than  $10^{-10}$ .

## 6.2 Energy calculations

Now that we have computed the wave-guide modes, we can solve (2.14) with  $u^{\text{inc}}$  equal to  $u_{j;l,+}$ . Figure 13 shows the resulting  $u$  and the total field. Using (6.4), we can compute the guided-mode components of  $u^{\text{out}}$  by

$$u_g^{\text{out}} = \left( \sum_j c_{j,-}^l u_{j;l,-} \right) \chi_{x_1 < 0} + \left( \sum_j c_{j,+}^r u_{j;r,+} \right) \chi_{x_1 > 0}. \quad (6.5)$$

The difference  $u_c^{\text{out}} := u^{\text{out}} - u_g^{\text{out}}$  represents the portion of the field that is radiated away from the junction. The components  $u_g^{\text{out}}$  and  $u_c^{\text{out}}$  are shown in Figure 13. This calculation shows that a much larger portion of the wave is transmitted than reflected. We can also see that a large portion is radiated away. This calculation represents the information in one column of the scattering matrix introduced in Section 2.3.

With these projections, we are able to determine how much power is sent into each wave-guide and how much is lost. Using the formulas from Section 2.3 we see that the transmitted power is  $P_r := \sum_j \xi_j^l |c_{j,+}^r|^2$ . The total reflected power is  $P_l := \sum_j \xi_j^l |c_{j,-}^l|^2$ . The total outgoing power is

$$P^{\text{out}} = P_r + P_l + P_{\text{rad}} := \lim_{R \rightarrow \infty} \Im \int_{|x|=R} \overline{u^{\text{out}}} \partial_r u^{\text{out}} R d\theta \quad (6.6)$$



$\nu$  is the outward normal to  $\Gamma$ . Hence the power lost to radiation is

$$P_{\text{rad}} = P^{\text{out}} - P_r - P_l. \quad (6.7)$$

This definition is slow to evaluate. If the incoming data is a single wave-guide mode,  $e^{i\xi_j^l x_1} v_j(x_2)$ , then Theorem 1 gives that

$$\xi_j^l = P_r + P_l + P_{\text{rad}}. \quad (6.8)$$

This formula gives us a much easier way to compute the radiated power, since  $P_r$  and  $P_l$  are easy to compute using (6.4). To verify that our computed solution satisfies this conservation law, we compute the integral (6.6) on the boundary of the box centered at the origin with side length 40. We discretize the integral using 500 Gauss-Legendre nodes on each side and found that the computed results satisfy (6.8) to 5 digits. To test that our solver satisfies (6.6), we compute  $P_{\text{rad}}$  using an equivalent integral and find

$$P_l/\xi_j^l = 0.03772, \quad P_r/\xi_j^l = 0.56841, \quad \text{and} \quad P_{\text{rad}}/\xi_j^l = 0.39388. \quad (6.9)$$

Since  $P_r + P_l + P_{\text{rad}} = 1.00001\xi_j^l$ , we see that our solver satisfies (6.8) to 5 digits.

## 7 Other examples

So far in this work, we have explored the solution of a single decomposable problem. In this section we explore a few other examples. The methods are presented without proof, but we do test each method with an analytic solution test analogous to the one performed in Section 5. In these examples the exterior wave number  $k = 1$ .

### 7.1 Terminating wave-guides

It is interesting to study how a wave scatters off of the end of a semi-infinite wave-guide. We can model this in the same framework as the matched wave-guide problem if we choose

$$q_r(\mathbf{x}) = (2^2 - 1)\chi_D(\mathbf{x}), \quad (7.1)$$

where  $D$  is a bounded region that determines the shape of the end of the wave-guide. The Green's function with this choice of  $q_r$  can be computed using the method described in Section 3 with  $\gamma = \partial D$ . As an example, we choose  $D$  to be the region in Figure 14a. By choosing  $D$  to be symmetric, we ensure that  $\mathcal{S}'_{q_r}$  and  $\mathcal{D}_{q_r}$  are still zero, which reduces the computational cost. We solve the resulting modified version of (2.14) to find the field generated by a wave-guide mode coming in from the left. The resulting total field is shown in Figure 14b. An analytic solution test shows that the solution is accurate to 6 digits everywhere away from  $\hat{\gamma}$  and the method described in Section 6.2 shows that the solution satisfies (6.8) to 6 digits.

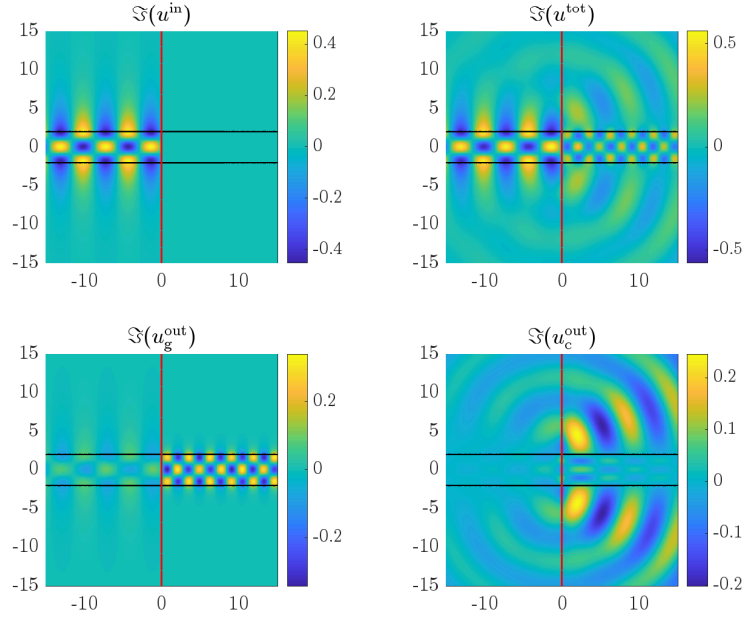
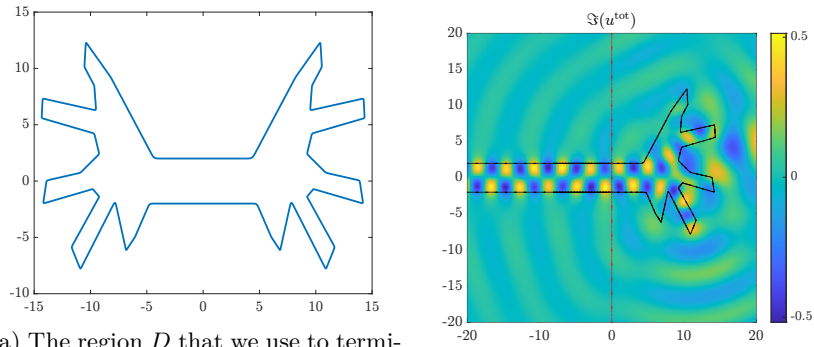


Figure 13: In this figure, we demonstrate how the solution can be decomposed into guided-mode and radiated components. The top two figures show the incoming and total fields. The bottom left figure shows the guided-mode component  $u_g^{\text{out}}$ . The bottom right shows the radiated part  $u_c^{\text{out}}$  computed as  $u^{\text{out}} - u_g^{\text{out}}$ .



(a) The region  $D$  that we use to terminate a wave-guide. We ensure that  $D$  is symmetric to reduce the number of terms in (2.14). (b) The resulting solution when  $u^{\text{inc}}$  is chosen to be a wave-guide mode of the left subdomain.

Figure 14: This figure shows our simulation of a terminating wave-guide.

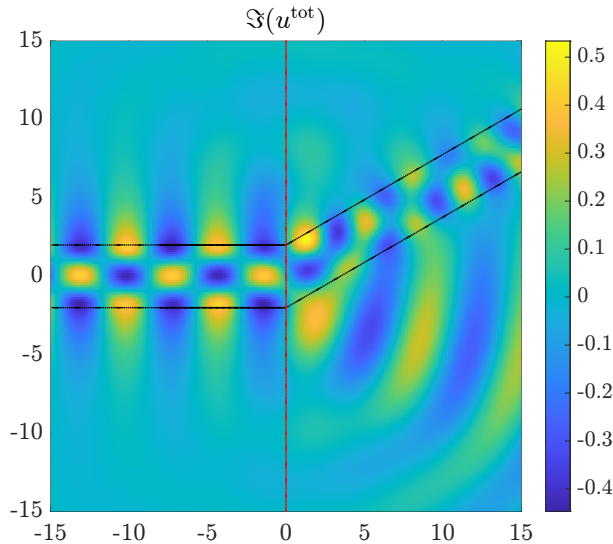


Figure 15: Our simulation of a bent wave-guide with  $u^{\text{inc}}$  chosen to be a wave-guide mode.

## 7.2 Bent Wave-guides

The algorithm described in previous sections can also be used to study the size of the field radiated when a corner is introduced in a wave-guide. To do this, we choose

$$q_r(\mathbf{x}) = (2^2 - 1)\chi_D(\mathbf{x}), \quad (7.2)$$

where  $D$  is a wave-guide tilted away from the positive  $x_1$ -axis by  $\pi/6$  radians, with width chosen to line up with the left wave-guide. The rotated wave-guide Green's function  $G_{q_r}$  can be computed in the same way as the other wave-guides. It should be noted, however, that as the wave-guide is rotated closer to the  $x_2$ -axis, the far-field region  $Z_F$  is pushed farther along  $\hat{\gamma}$  and so the computation becomes more costly.

With this code, we computed the field generated by an incoming wave-guide mode. The resulting total field is shown in Figure 15. An analytic solution tests gives that the solution is accurate to 4 digits everywhere away from the  $\hat{\gamma}$  and the method described in Section 6.2 shows that the solution satisfies (6.8) to 5 digits.

## 7.3 A Wave-guide junction

In this section, we describe how to simulate a junction between more than 2 wave-guides. We model the case where a single wave-guide is split into two parallel wave-guides (see Figure 16). In this case, we split the domain into three regions: the left and right wave-guides, and a compact transition region.

For illustrative purposes, we focus on the case where all wave-guides have the same wave-number. This method could be extended to the case where wavenumber changes smoothly using standard integral equation techniques. To solve this problem, we compute the domains Green's functions for the left and center domains using the techniques described in Sections 3 and 7.1. The domain with two parallel wave-guides can be handled using the same technique, except that  $\tilde{\gamma}$  has four disjoint pieces. We use these Green's function to represent the solution  $u$  as

$$u_{l,m,r} = \mathcal{S}_{q_{l,m,r}}[\sigma] + \mathcal{D}_{q_{l,m,r}}[\tau], \quad (7.3)$$

where the integral operators are now supported on the union of the all the domain boundaries (the red lines in Figure 16). If we plug this representation into the continuity conditions along those boundaries, then we arrive at an integral equation that is equivalent to (2.14). In this case, however, the operators  $\mathcal{D}_{q_{l,m,r}}$  and  $\mathcal{S}'_{q_{l,m,r}}$  are no longer zero on the boundary of the compact region.

We discretize this integral equation using similar discretization techniques to those described, and solve the system to compute the field generated by an incoming wave-guide mode. The resulting field is shown in Figure 16. An analytic solution tests indicates that the solution is accurate to 6 digits everywhere away from the interfaces and the method described in Section 6.2 shows that the solution satisfies (6.8) to 5 digits.

With this solver, we can tune the input signal to maximize the power sent down either channel. To do this, we must find the wave-guide modes for a pair of parallel channels. It is not hard to show that these wave-guide modes are perturbations of the modes for a single wave-guide. Indeed, if the separation of the wave-guides is  $2h$ , then the wave-guide frequencies are the roots of

$$f_e(\xi) = \left[ k_{1;l,r}^2 - \xi^2 + (k^2 - \xi^2) \tanh \left( h\sqrt{k^2 - \xi^2} \right) \right] \sin \left( 2d\sqrt{k_{1;l,r}^2 - \xi^2} \right) - \left( 1 + \tanh \left( h\sqrt{k^2 - \xi^2} \right) \right) \sqrt{\xi^2 - k^2} \sqrt{k_{1;l,r}^2 - \xi^2} \cos \left( 2d\sqrt{k_{1;l,r}^2 - \xi^2} \right) \quad (7.4)$$

if  $v_{r,n}$  is even or

$$f_o(\xi) = \left[ k_{1;l,r}^2 - \xi^2 + (k^2 - \xi^2) \coth \left( h\sqrt{k^2 - \xi^2} \right) \right] \sin \left( 2d\sqrt{k_{1;l,r}^2 - \xi^2} \right) - \left( 1 + \coth \left( h\sqrt{k^2 - \xi^2} \right) \right) \sqrt{\xi^2 - k^2} \sqrt{k_{1;l,r}^2 - \xi^2} \cos \left( 2d\sqrt{k_{1;l,r}^2 - \xi^2} \right), \quad (7.5)$$

if it is odd. The functions  $f_e$  and  $f_o$  are both perturbations of (6.2). The resulting modes are shown in Figure 17. With these modes in hand, we can build the scattering matrix using the method from Section 6. Using a singular value decomposition of the scattering matrix, we pick  $u^{\text{inc}}$  to be the combination of modes that maximizes the power in the upper channel. The resulting solution is shown in Figure 18. Using this combination, 98.32% of the incoming power is sent into the upper channel, 0.27% is sent to the lower channel, 0.015% is reflected, and 1.40% is radiated, which shows that energy is conserved to 4 significant digits.

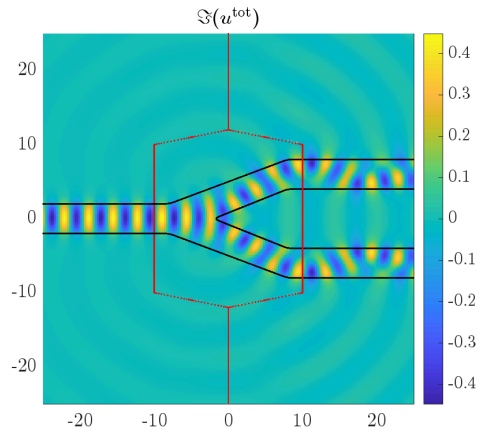


Figure 16: Simulation of a wave-guide junction.

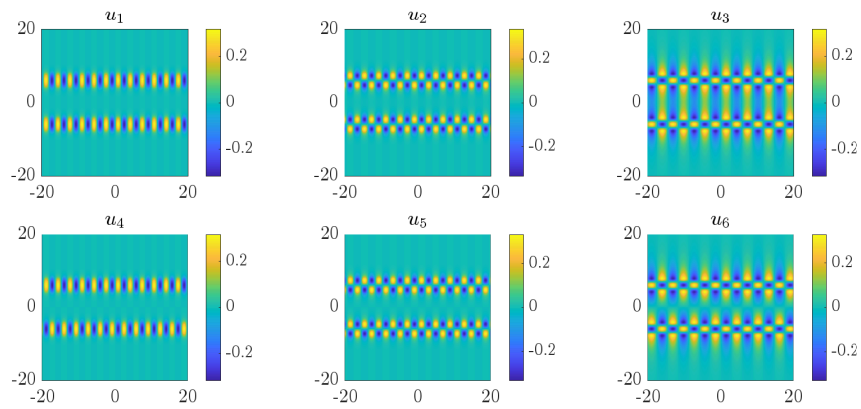


Figure 17: The wave-guide modes for the two parallel wave-guides used in Figure 16.

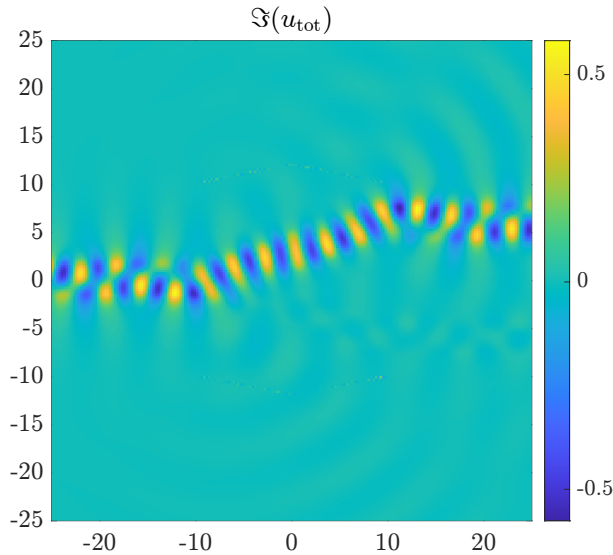


Figure 18: The combination of incoming wave-guide modes that sends the greatest power to the upper wave-guide.

#### 7.4 Dirichlet Wave-guides

As a final example, we consider the case where Dirichlet boundary conditions are imposed on the edges of the wave-guides. To compute the Green's function for a Dirichlet wave-guide, we use different methods, depending on the location of  $\mathbf{x}$  and  $\mathbf{y}$ . First, if  $\mathbf{x}$  and  $\mathbf{y}$  are not in the same section of the wave-guide, the Green's function is zero. Secondly, if  $\mathbf{x}$  and  $\mathbf{y}$  are both above or both below the wave-guide, then Green's function can be computed by placing an image charge at the reflection of  $\mathbf{y}$  in the closer edge of the wave-guide. For the final case, where  $\mathbf{x}$  and  $\mathbf{y}$  are inside the wave-guide, we compute the Green's function by solving an integral equation on the boundary of the wave-guide. Specifically, we suppose that

$$G_q^{\text{out}} = \mathcal{D}_k[\rho], \quad (7.6)$$

where the integral operator is supported on the boundary of the wave-guide. Plugging this into the boundary condition  $G_q^{\text{inc}} + G_q^{\text{out}} = 0$  on that boundary gives a second kind integral equation for  $\rho$ . We solve this integral equation using the same coordinate complexification and discretization techniques described above.

We can use this Green's function to simulate the case where the Dirichlet wave-guide ends without a cap. To make this simulation, we choose the left subdomain to be a Dirichlet wave-guide and the right subdomain to be the Helmholtz equation with Dirichlet boundary conditions imposed on two line segments that form the end of the pipe. By introducing these line segments, we move the corner singularity at the ends of the pipe away from the  $x_2$ -axis, which

ensures that the densities in the equivalent of (2.14) are piecewise smooth.

To find the Green's function for the right system, we must solve the so-called open arc problem. These problems are interesting in their own right and a lot of work has been done towards their accurate solution, see the references in [25]. In this paper, we build a simple solver for illustrative purposes. We describe our algorithm in the case that Dirichlet boundary conditions are applied on the line segment  $[-1, 1] \times \{0\}$ . More line segments can be added easily.

To find the Green's function for this scattering problem, we use the representation

$$G_{q_r}^{\text{out}} = \mathcal{S}_k[\rho], \quad (7.7)$$

where  $\mathcal{S}_k$  is an integral operator supported on the line segment. Plugging this representation into the Dirichlet boundary conditions leads to the first kind integral equation

$$\mathcal{S}_k[\rho] = -G_{q_r}^{\text{inc}}. \quad (7.8)$$

In [25] it was observed that the solution to (7.8) has an inverse square root singularity at each end of the line segment. We therefore introduce the scaled density

$$\tilde{\rho}(t) = \rho(t)\sqrt{1-t^2}, \quad (7.9)$$

which can be expected to be smooth up to  $t = \pm 1$ . If we plug this definition into (7.8) we see that  $\tilde{\rho}$  solves

$$\int_{-1}^1 G_k((t, 0); (t', 0)) \frac{\tilde{\rho}(t')}{\sqrt{1-(t')^2}} dt' = -G_{q_r}^{\text{inc}}((t, 0)). \quad (7.10)$$

The singularity in (7.10) can be removed with the change of variables  $t = \cos u$ :

$$\int_0^\pi G_k((\cos u, 0); (\cos u', 0)) \tilde{\rho}(\cos u') du' = -G_{q_r}^{\text{inc}}((\cos u, 0)), \quad (7.11)$$

Since this change of variables has removed the singularity, this equation can be discretized with a few equally sized Gauss-Legendre panels.

As a first kind equation, (7.11) is poorly conditioned when it is finely discretized. For illustrative purposes, however, we need only a fairly coarse discretization, and so the condition number is bounded by  $4 \times 10^3$ .

By using the methods described above to compute  $G_{q_l}$  and  $G_{q_r}$  we can reduce to solving an integral equation on the line dividing the two subdomains. Figure 19 shows the resulting solution generated by a point source at  $(-21, 0)$ . An analytic solution test indicates that the solution is accurate to 6 digits everywhere away from  $\tilde{\gamma}$ .

We can also use this technique to simulate the transmission of a wave between two nearby Dirichlet wave-guides. In this case, we split the problem into three regions. On either side, we have a Dirichlet wave-guide. In the middle region, we apply Dirichlet boundary conditions on a few line intervals. To solve the problem, we impose continuity conditions on two lines parallel to the  $x_2$ -axis and solve the resulting system of integral equations. The resulting solution

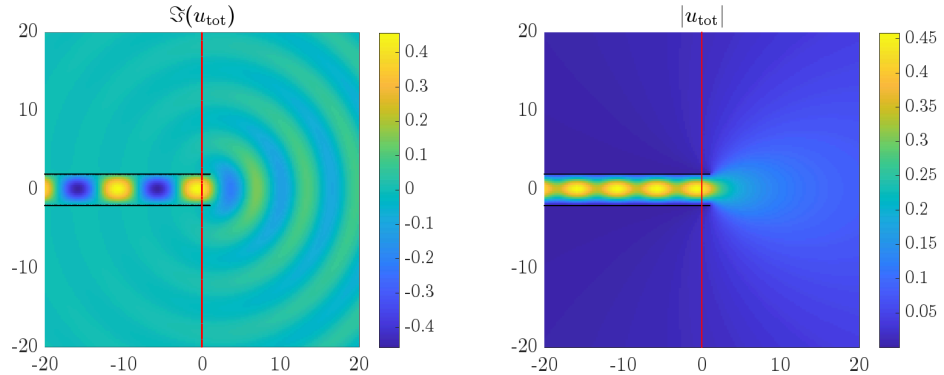


Figure 19: This figures show the imaginary part and the modulus of the solution of a terminate Dirichlet wave-guide.

generated by a point source at  $(-31, 0)$  is shown in Figure 20. An analytic solution test indicates that the solution is accurate to 5 digits everywhere away from  $\tilde{\gamma}$ .

## 8 Conclusion

In this paper we have introduced the class of decomposable scattering problems on unbounded domains. We begin with an operator  $L$ . A problem is decomposable if the computational domain can be split up into pieces, such that, in each unbounded component, the operator  $L$  has an outgoing fundamental solution that can be computed efficiently. We show how to use the method of fundamental solutions to reduce the problem to systems of integral equations on the union of the domain boundaries. The method becomes practicable if the domain fundamental solutions have analytic continuations that allow the resulting integral equation to be solved using coordinate complexification and standard integral equations techniques.

When implemented naively, these integral equation methods can be slow, as the evaluations of the kernel functions of the domain fundamental solutions require solving a PDE. We therefore introduce a method for building compressed representations of these domain fundamental solutions, which allow us to solve these integral equations efficiently.

This method is applied to the case of 2 semi-infinite wave-guides meeting along a common perpendicular line. We conclude with a number of other examples of decomposable problems, including a wave-guide with a Y-junction, a wave-guide with a bend, and Dirichlet wave-guides. In future works, we plan



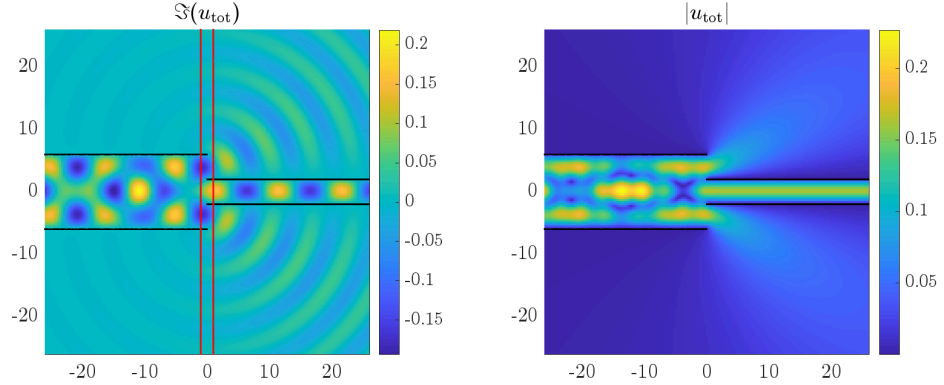


Figure 20: This figures show the imaginary part and the modulus of the solution of two Dirichlet wave-guides placed end to end.

to provide a rigorous justification for our use of coordinate complexification to solve (2.14) and to extend this method to other decomposable problems.

## A Energy Conservation for Open Wave-guides

In this appendix we give the proof of Theorem 1, which shows that the scattering matrix, at a fixed real frequency, for an open wave-guide is a unitary map. The argument applies to any 2-dimensional wave-guide as modeled by a potential of the form given in (1.1). This analysis uses concepts introduced in [19].

To begin we let  $\overline{\mathbb{R}^2}$  denote the radial compactification of  $\mathbb{R}^2$ , with  $\partial\overline{\mathbb{R}^2} \simeq S^1$ , the unit circle, see [19]. Suppose that  $q(\mathbf{x})$  defines an open wave-guide in the plane. This means that there is a collection of distinct directions  $\mathcal{C} = \{\omega_1, \dots, \omega_N\} \subset \partial\overline{\mathbb{R}^2} \simeq S^1$  that define the channel ends, and real valued, compactly supported functions of 1-variable  $\{q_1, \dots, q_N\}$ , so that

$$q(\mathbf{x}) = q_0(\mathbf{x}) + \sum_{j=1}^N q_j(\mathbf{x} - \langle \mathbf{x}, \omega_j \rangle \omega_j) \varphi_+(r_j \langle \mathbf{x}, \omega_j \rangle) \quad (\text{A.1})$$

where  $q_0 \in L^\infty(\mathbb{R}^2)$  is compactly supported and  $\varphi_+ \in C^\infty(\mathbb{R})$  is a monotone function with

$$\varphi_+(t) = \begin{cases} 0 & \text{for } t < 1, \\ 1 & \text{for } t > 2. \end{cases} \quad (\text{A.2})$$

The operator  $\Delta + q$  is self adjoint with domain  $H^2(\mathbb{R}^2)$ .

We are then interested in solutions,  $u$  to

$$(\Delta + q(\mathbf{x}) + k^2)u(\mathbf{x}) = f(\mathbf{x}) \in \mathcal{S}(\mathbb{R}^2), \quad (\text{A.3})$$

with asymptotic expansions at infinity. By this we mean that

$$u(r\omega) = \frac{e^{ikr}}{r^{\frac{1}{2}}} [a_+(\omega) + O(r^{-1})] + \frac{e^{-ikr}}{r^{\frac{1}{2}}} [a_-(\omega) + O(r^{-1})] \quad (\text{A.4})$$

with

$$a_{\pm} \in C^\infty(S^1 \setminus \{\omega_1, \dots, \omega_N\}) \cap L^\infty(S^1).$$

In addition we assume that in a conic neighborhood,  $V_j$  of each channel end,  $\omega_j \in \mathcal{C}$ , in which we can write

$$u(\mathbf{x}) = u_c^j(\mathbf{x}) + u_g^j(\mathbf{x}) \text{ for } \mathbf{x} \in V_j, \quad (\text{A.5})$$

where  $u_g^j$  is a sum of the wave-guide modes,  $\{v_l^j : l = 1, \dots, M_j\}$ , for the bi-infinite open wave guide defined by  $\Delta + q_j(\mathbf{x} - \langle \mathbf{x}, \omega_j \rangle \omega_j) + k^2$ , and  $u_c^j(\mathbf{x})$  is the contribution from the continuous spectrum. It satisfies

$$u_c(r\omega) = O(r^{-\frac{1}{2}}), \quad (\text{A.6})$$

uniformly for  $r\omega \in V_j$ . The estimate in (A.6) follows by combining the estimates in (95), (209) and (280) from [17], using the uniformity of the estimate in (280) as  $\theta_{\pm} \rightarrow 0^{\pm}$ . For  $l = 1, \dots, M_j$ ,

$$\begin{aligned} \lim_{x_1 \rightarrow \infty} \int_{-\infty}^{\infty} u_c(x_1, x_2) \overline{v_l^j(x_2)} dx_2 = 0 \text{ and} \\ \lim_{x_1 \rightarrow \infty} \int_{-\infty}^{\infty} \partial_{x_1} u_c(x_1, x_2) \overline{v_l^j(x_2)} dx_2 = 0, \end{aligned} \quad (\text{A.7})$$

where we have chosen coordinates so that  $\omega_j = (1, 0)$ .

Using results from [16, 17] and the formula in Appendix B, these asymptotics have been established in the  $2d$ -case. More generally this follows from the fact that an incoming or outgoing solution to  $(\Delta + q + k^2)u = 0$  can be written in a conic neighborhood,  $V_j$ , of  $\omega_j$  as an integral over  $\partial V_j$  with respect to the outgoing resolvent kernels,  $(\Delta + q_j + k^2 + i0)^{-1}$ . This is proved in Appendix B for certain kinds of incoming data.

We now define  $\{\Omega_R, : R > 0\}$ , a family of domains that exhaust  $\mathbb{R}^2$  as  $R \rightarrow \infty$ , adapted to the wave-guide geometry (Figure 21). For an  $0 < \epsilon < \frac{1}{2}$  we let

$$\theta_R = R^{\epsilon-1}. \quad (\text{A.8})$$

For  $\omega_j = (\cos \theta_j, \sin \theta_j)$ , let  $C_{j,R}$  be the truncated cone:

$$\begin{aligned} C_{j,R} = \{ \lambda r(\cos(\theta_j + \theta_R), \sin(\theta_j + \theta_R)) + \\ (1 - \lambda)r(\cos(\theta_j - \theta_R), \sin(\theta_j - \theta_R)) : r \in [0, R], \lambda \in [0, 1] \}. \end{aligned} \quad (\text{A.9})$$

A point  $\mathbf{x} = r(\cos \theta, \sin \theta) \in \Omega_R$  if

$$r < R \text{ and } \min\{|\theta - \theta_j| : j = 1, \dots, N\} > \theta_R \text{ or } \mathbf{x} \in C_{j,R} \text{ for some } j; \quad (\text{A.10})$$

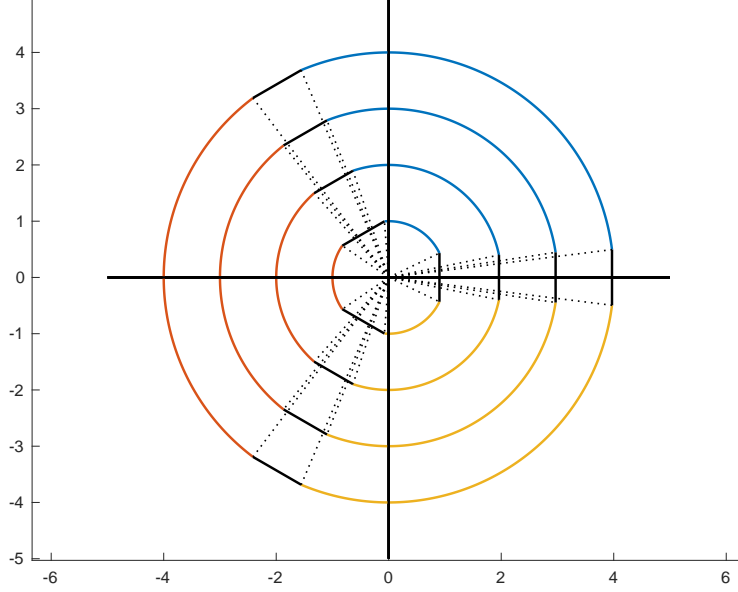


Figure 21: A collection of domains  $\Omega_{R_j}$  for a wave-guide with 3 channels.

set  $\Gamma_R = \partial\Omega_R \setminus \cup_{j=1}^N \partial C_{j,R}$ , and let  $\partial_o C_{j,R} = \partial C_{j,R} \cap \partial\Omega_R$ , denote the *outer* boundary of  $C_{j,R}$ . Examples of  $\Omega_R$ , for a range of  $R$ , are shown in Figure 21.

We now show that the incoming energy equals the outgoing energy using a fairly standard argument, similar to the proof of this fact given in [31]. Suppose that we have two solutions of

$$(\Delta + q + k^2)u_m = f_m \in \mathcal{S}(\mathbb{R}^2), \quad m = 1, 2, \quad (\text{A.11})$$

with asymptotic expansions

$$u_m(r\omega) = \frac{e^{irk}}{\sqrt{r}} a_{m+}(\omega) + \frac{e^{-irk}}{\sqrt{r}} a_{m-}(\omega) + o(r^{-\frac{1}{2}}), \quad \text{for } \omega \notin \{\omega_j\}. \quad (\text{A.12})$$

The coefficients  $\{a_{j\pm}(\omega)\}$  remain bounded as  $\omega$  approaches  $\omega_j$  from above and below, and that is what is understood here. If we choose coordinates so the  $\omega_j = (1, 0)$ , then in a conic neighborhood,  $V_j \in \partial\overline{\mathbb{R}^2}$  we also have the expansion

$$u_m(x_1, x_2) = \sum_{l=1}^{M_j} \left[ a_{ml}^j e^{i\xi_l^j x_1} v_l^j(x_2) + b_{ml}^j e^{-i\xi_l^j x_1} v_l^j(x_2) \right] + O(x_1^{-\frac{1}{2}}), \quad \text{as } \pm x_1 \rightarrow \infty. \quad (\text{A.13})$$

The finite sum is just  $u_{mg}(x_1, x_2)|_{V_j}$ . We assume that the exponentially decaying transverse components of the wave-guide modes,  $\{v_l^j(x_2)\}$ , are normalized

so that

$$\int_{-\infty}^{\infty} v_l^j(x_2) \overline{v_k^j(x_2)} dx_2 = \delta_{lk}. \quad (\text{A.14})$$

Following Melrose in [31], we begin with the bi-linear relation

$$\begin{aligned} & \lim_{R \rightarrow \infty} \int_{\Omega_R} [u_1 \cdot \overline{f_2} - f_1 \cdot \overline{u_2}] d\mathbf{x} \\ &= \lim_{R \rightarrow \infty} \int_{\Omega_R} [u_1 \cdot \overline{(\Delta + q + k^2)u_2} - (\Delta + q + k^2)u_1 \cdot \overline{u_2}] d\mathbf{x} \\ &= \lim_{R \rightarrow \infty} \int_{\partial\Omega_R} [u_1 \cdot \overline{\partial_\nu u_2} - \partial_\nu u_1 \cdot \overline{u_2}] ds. \end{aligned} \quad (\text{A.15})$$

Stokes' Theorem is used to go from the second to the third line; here  $\nu$  is the outer unit normal to  $\partial\Omega_R$ .

First consider the contribution of  $\Gamma_R$ . For this part of  $\partial\Omega_R$  we use the expansions in (A.12), which gives

$$\int_{\Gamma_R} [u_1 \cdot \overline{\partial_r u_2} - \partial_r u_1 \cdot \overline{u_2}] ds = 2ik \int_{\Gamma_R} [a_{1-}(\omega) \overline{a_{2-}(\omega)} - a_{1+}(\omega) \overline{a_{2+}(\omega)}] d\omega + o(1). \quad (\text{A.16})$$

Given our assumptions on the coefficients  $a_\pm$ , this term converges, as  $R \rightarrow \infty$ , to

$$2ik \int_{S^1} [a_{1-}(\omega) \overline{a_{2-}(\omega)} - a_{1+}(\omega) \overline{a_{2+}(\omega)}] d\omega. \quad (\text{A.17})$$

We now analyze the contributions of the channel ends. Fix a  $j \in \{1, \dots, N\}$  and choose coordinates so that  $\omega_j = (1, 0)$ . The contribution of outer portion of  $\partial C_{j,R}$  takes the form

$$\begin{aligned} & \int_{\partial_o C_{j,R}} [u_1 \cdot \overline{\partial_\nu u_2} - \partial_\nu u_1 \cdot \overline{u_2}] ds \\ &= \int_{-R \sin \theta_R}^{R \sin \theta_R} [u_1 \cdot \overline{\partial_{x_1} u_2} - \partial_{x_1} u_1 \cdot \overline{u_2}] (R \cos \theta_R, x_2) dx_2 \\ &= \int_{-R \sin \theta_R}^{R \sin \theta_R} [u_{1g} \cdot \overline{\partial_{x_1} u_{2g}} - \partial_{x_1} u_{1g} \cdot \overline{u_{2g}}] (R \cos \theta_R, x_2) dx_2 + O(R^{-\frac{1}{2}} + R^{\epsilon-1}). \end{aligned} \quad (\text{A.18})$$

To go from the second to the third line we use the assumptions about the asymptotic expansion to see that, e.g.

$$u_{1c} \overline{\partial_{x_1} u_{2c}}(x_1, x_2) = O(x_1^{-1}), \quad u_{1g} \overline{\partial_{x_1} u_{2c}}(x_1, x_2) = O(x_1^{-\frac{1}{2}} e^{-\alpha|x_2|}), \text{ etc.},$$

for an  $\alpha > 0$ . As  $R \sin \theta_R \sim R^\epsilon$  for some  $\epsilon < \frac{1}{2}$ , the estimate follows.

To compute the contribution of the remaining term we use the expansions in (A.13). The fact that  $R \sin \theta_R \rightarrow \infty$  and the orthogonality relations in (A.14)

imply that

$$\lim_{R \rightarrow \infty} \int_{-R \sin \theta_R}^{R \sin \theta_R} [u_{1g} \cdot \overline{\partial_{x_1} u_{2g}} - \partial_{x_1} u_{1g} \cdot \overline{u_{2g}}] (R \cos \theta_R, x_2) dx_2 = 2i \sum_{l=1}^{M_j} \xi_l^j [b_{1l}^j \overline{b_{2l}^j} - a_{1l}^j \overline{a_{2l}^j}]. \quad (\text{A.19})$$

Assembling the complete formula we see that

$$\int_{\mathbb{R}^2} [u_1 \cdot \overline{f_2} - f_1 \cdot \overline{u_2}] d\mathbf{x} = 2ik \int_{S^1} [a_{1-}(\omega) \overline{a_{2-}(\omega)} - a_{1+}(\omega) \overline{a_{2+}(\omega)}] d\omega + 2i \sum_{j=1}^N \sum_{l=1}^{M_j} \xi_l^j [b_{1l}^j \overline{b_{2l}^j} - a_{1l}^j \overline{a_{2l}^j}]. \quad (\text{A.20})$$

Of particular interest is the case  $u_1 = u_2$  and  $f_1 = f_2 = 0$ ; in this case we see that

$$k \int_{S^1} |a_-(\omega)|^2 d\omega + \sum_{j=1}^N \sum_{l=1}^{M_j} \xi_l^j |b_l^j|^2 = k \int_{S^1} |a_+(\omega)|^2 d\omega + \sum_{j=1}^N \sum_{l=1}^{M_j} \xi_l^j |a_l^j|^2. \quad (\text{A.21})$$

This completes the proof of Theorem 1.

The scattering map in this case carries the coefficients of the incoming asymptotics to those of the outgoing asymptotics; it is given by

$$S(k) : \left( \sqrt{k} a_-(\omega), \left[ \sqrt{\xi_l^j} b_l^j : l = 1, \dots, M_j, j = 1, \dots, N \right] \right) \mapsto \left( \sqrt{k} a_+(\omega), \left[ \sqrt{\xi_l^j} a_l^j : l = 1, \dots, M_j, j = 1, \dots, N \right] \right). \quad (\text{A.22})$$

It follows from (A.21) that  $S(k)$  is a unitary map.

In the simplest case of two semi-infinite wave-guides meeting along common perpendicular line we have left and right wave-guide modes

$$\{v_j^l(x_2) e^{\pm i \xi_j^l x_1} : j = 1, \dots, N_l\}, \quad \{v_j^r(x_2) e^{\pm i \xi_j^r x_1} : j = 1, \dots, N_r\}.$$

For definiteness we take  $\xi_j^{l,r} > 0$ ; normalized as before. In this case the unitarity statement is:

$$k \int_0^{2\pi} |a_-(\omega)|^2 d\omega + \sum_{j=1}^{N_r} \xi_j^r |b_j^r|^2 + \sum_{j=1}^{N_l} \xi_j^l |b_j^l|^2 = k \int_0^{2\pi} |a_+(\omega)|^2 d\omega + \sum_{j=1}^{N_r} \xi_j^r |a_j^r|^2 + \sum_{j=1}^{N_l} \xi_j^l |a_j^l|^2 \quad (\text{A.23})$$

## B Representation of Solutions Near to Channel Ends

We show that the outgoing part of a solution to  $(\Delta + q + k^2)u = 0$  has a representation in a conic neighborhood of each channel end in terms of the bi-infinite wave-guide L.A.P. resolvent  $(\Delta + q_j + k^2 + i0)^{-1}$ , which leads to the representations in (A.5). In this appendix we assume that the incoming part of  $u$  comes from a wave-guide mode. Similar arguments will apply with other kinds of incoming data. We carry out this argument in  $d$ -dimensions.

Let  $v_l^j(\mathbf{x}')e^{-i\xi_l^j x_1}$  be an incoming wave guide mode associated to the  $j$ th channel, where we have chosen coordinates so that  $\omega_j = (1, 0, \dots, 0)$ . We choose a  $C^\infty$  conic cut-off

$$\Psi_\delta^j(r\omega) = \varphi_+(r)\psi_\delta(\langle \omega, \omega_j \rangle), \quad (\text{B.1})$$

where  $\varphi_+(r) = 0$ , for  $r < r_j$  and 1 for  $r > 2r_j$ , and

$$\psi_\delta(t) = \begin{cases} 1 & \text{for } t > 1 - \delta, \\ 0 & \text{for } t \ll 1 - 2\delta. \end{cases} \quad (\text{B.2})$$

Set  $\tilde{u}_j(\mathbf{x}) = \Psi_\delta^j(\mathbf{x})v_l^j(\mathbf{x}')e^{-i\xi_l^j x_1}$ , and observe that

$$w_j = (\Delta + q + k^2)\tilde{u}_j = 2\nabla\Psi_\delta^j \cdot \nabla(v_l^j(\mathbf{x}')e^{-i\xi_l^j x_1}) + \Delta(\Psi_\delta^j)v_l^j(\mathbf{x}')e^{-i\xi_l^j x_1} \in \mathcal{S}(\mathbb{R}^d). \quad (\text{B.3})$$

This follows as the terms  $\nabla\Psi_\delta^j$  and  $\Delta\Psi_\delta^j$  are supported near a cone with axis along the positive  $x_1$ -axis, and  $v_l^j(\mathbf{x}')$  decays exponentially in this set. This shows that  $w_j$  is in the domain of the L.A.P. resolvent  $R(k^2 + i0) = (\Delta + q + k^2)^{-1}$  and therefore if we let

$$\tilde{w}_j = (\Delta + q + k^2)^{-1}w_j, \quad (\text{B.4})$$

then  $\tilde{w}_j$  is outgoing, and the function

$$u_{jl}^{\text{tot}} = \tilde{u}_j(\mathbf{x}) - \tilde{w}_j(\mathbf{x}) \quad (\text{B.5})$$

satisfies  $(\Delta + q + k^2)u_{jl}^{\text{tot}} = 0$ . By results in [44], the fact that  $\tilde{w}_j$  is outgoing implies that it has an expansion of the form

$$\tilde{w}_j(r\omega) = \frac{e^{ikr}}{r^{\frac{d-1}{2}}} \cdot \sum_{m=0}^{\infty} \frac{a_m^+(\omega)}{r^m}, \quad (\text{B.6})$$

where  $a_m^+ \in C^\infty(\partial\overline{\mathbb{R}^d} \setminus \{\omega_j : j = 1, \dots, N\})$ .

It is also true that there is a conic neighborhood  $\tilde{V}_j$  of  $\omega_j$  in which

$$(\Delta + q_j + k^2)\tilde{w}_j(\mathbf{x}) = 0. \quad (\text{B.7})$$

By choosing  $\delta' < \delta$  we can arrange to have  $\text{supp } \Psi_{\delta'}^j \subset \tilde{V}_j$ ; as  $\Psi_{\delta'}^j$  depends only on  $\omega$ , for large enough  $r$ , we see that

$$f_j = (\Delta + q_j + k^2)[\Psi_{\delta'}^j \tilde{w}_j] = 2\nabla\Psi_{\delta'}^j \cdot \nabla\tilde{w}_j + (\Delta\Psi_{\delta'}^j)\tilde{w}_j = O(|\mathbf{x}|^{-\frac{d+3}{2}}), \quad (\text{B.8})$$

which shows that  $f_j$  is in the domain of the  $j$ th L.A.P. resolvent  $(\Delta + q_j + i0)^{-1}$ .

If we let  $g_j = (\Delta + q_j + i0)^{-1} f_j$ , then  $g_j$  is the *unique* outgoing solution to

$$(\Delta + q_j + k^2)g_j = f_j. \quad (\text{B.9})$$

But  $\Psi_{\delta'}^j \tilde{w}_j$  is also an outgoing solution to this equation, and therefore  $g_j = \Psi_{\delta'}^j \tilde{w}_j$ , which implies that

$$\begin{aligned} \Psi_{\delta'}^j \tilde{w}_j(\mathbf{x}) &= \lim_{R \rightarrow \infty} \int_{B_R} R_j(k^2 + i0)(\mathbf{x}; \mathbf{y})(\Delta + q_j + k^2)\Psi_{\delta'}^j \tilde{w}_j(\mathbf{y}) d\mathbf{y} \\ &= \lim_{R \rightarrow \infty} \int_{\partial B_R} [R_j(k^2 + i0)(\mathbf{x}; \mathbf{y})\partial_r \Psi_{\delta'}^j \tilde{w}_j - \partial_r R_j(k^2 + i0)(\mathbf{x}; \mathbf{y})\Psi_{\delta'}^j \tilde{w}_j] dS_{\mathbf{y}} \\ &\quad + \Psi_{\delta'}^j \tilde{w}_j(\mathbf{x}). \end{aligned} \quad (\text{B.10})$$

Therefore

$$\lim_{R \rightarrow \infty} \int_{\partial B_R} [R_j(k^2 + i0)(\mathbf{x}; \mathbf{y})\partial_r \Psi_{\delta'}^j \tilde{w}_j - \partial_r R_j(k^2 + i0)(\mathbf{x}; \mathbf{y})\Psi_{\delta'}^j \tilde{w}_j] dS_{\mathbf{y}} = 0. \quad (\text{B.11})$$

Away from the channel ends this statement follows from (B.6), but is non-trivial near to  $\omega_j$ . Note also that  $\text{supp}(\Psi_{\delta'}^j \tilde{w}_j) \subset \tilde{V}_j$ , which is disjoint from  $\mathcal{C} \setminus \{\omega_j\}$ .

With this understood we can now use Green's formula in the cone  $\tilde{V}_j$  to conclude that, for  $\mathbf{x} \in \tilde{V}_j$ ,

$$\begin{aligned} 0 &= \lim_{R \rightarrow \infty} \int_{\tilde{V}_j \cap B_R} R_j(k^2 + i0)(\mathbf{x}; \mathbf{y})(\Delta + q_j + k^2)\tilde{w}_j(\mathbf{y}) d\mathbf{y} \\ &= \lim_{R \rightarrow \infty} \left[ \int_{\partial \tilde{V}_j \cap B_R} [R_j(k^2 + i0)(\mathbf{x}; \mathbf{y})\partial_{\nu} \tilde{w}_j(\mathbf{y}) - \partial_{\nu} R_j(k^2 + i0)(\mathbf{x}; \mathbf{y})\tilde{w}_j(\mathbf{y})] dS_{\mathbf{y}} + \right. \\ &\quad \left. \int_{\tilde{V}_j \cap \partial B_R} [R_j(k^2 + i0)(\mathbf{x}; \mathbf{y})\partial_{\nu} \tilde{w}_j(\mathbf{y}) - \partial_{\nu} R_j(k^2 + i0)(\mathbf{x}; \mathbf{y})\tilde{w}_j(\mathbf{y})] dS_{\mathbf{y}} \right] + \tilde{w}_j(\mathbf{x}) \\ &= \int_{\partial \tilde{V}_j} [R_j(k^2 + i0)(\mathbf{x}; \mathbf{y})\partial_{\nu} \tilde{w}_j(\mathbf{y}) - \partial_{\nu} R_j(k^2 + i0)(\mathbf{x}; \mathbf{y})\tilde{w}_j(\mathbf{y})] dS_{\mathbf{y}} + \tilde{w}_j(\mathbf{x}). \end{aligned} \quad (\text{B.12})$$

It is easy to see that the integral over  $\partial \tilde{V}_j$  is absolutely convergent, and above we showed that the integral over  $\tilde{V}_j \cap \partial B_R$  goes to zero as  $R \rightarrow \infty$ . This gives the desired representation formula:

$$\tilde{w}_j(\mathbf{x}) = \int_{\partial \tilde{V}_j} [\partial_{\nu} R_j(k^2 + i0)(\mathbf{x}; \mathbf{y})\tilde{w}_j(\mathbf{y}) - R_j(k^2 + i0)(\mathbf{x}; \mathbf{y})\partial_{\nu} \tilde{w}_j(\mathbf{y})] dS_{\mathbf{y}}, \quad (\text{B.13})$$

for  $\mathbf{x} \in \tilde{V}_j$ .

All that is required to obtain the representation in (A.5) is the description of the bi-infinite wave-guide, L.A.P. resolvent kernels,  $R_j(k^2 + i0)(\mathbf{x}; \mathbf{y})$ , as the sums of a continuous spectral part and the wave-guide contribution. In the 2d-case this is given in [16, 17].

## References

- [1] F. J. Agocs and A. H. Barnett. Trapped acoustic waves and raindrops: high-order accurate integral equation method for localized excitation of a periodic staircase. *Journal of Computational Physics*, page 113383, 2024.
- [2] B. Alpert, L. Greengard, and T. Hagstrom. Nonreflecting boundary conditions for the time-dependent wave equation. *Journal of Computational Physics*, 180(1):270–296, 2002.
- [3] T. Askham, M. Rachh, M. O’Neil, J. Hoskins, D. Fortunato, S. Jiang, F. Fryklund, T. Goodwill, H. Yang, and H. Zhu. chunkIE: a MATLAB integral equation toolbox. <https://github.com/fastalgorithms/chunkie>, 2024.
- [4] E. Bécache and M. Kachanovska. Stability and convergence analysis of time-domain perfectly matched layers for the wave equation in waveguides. *SIAM Journal on Numerical Analysis*, 59(4):2004–2039, 2021.
- [5] A.-S. Bonnet-Ben Dhia, S. N. Chandler-Wilde, and S. Fliss. On the half-space matching method for real wavenumber. *SIAM Journal on Applied Mathematics*, 82(4):1287–1311, 2022.
- [6] A.-S. Bonnet-Ben Dhia, S. N. Chandler-Wilde, S. Fliss, C. Hazard, K.-M. Perfekt, and Y. Tjandrawidjaja. The complex-scaled half-space matching method. *SIAM Journal on Mathematical Analysis*, 54(1):512–557, 2022.
- [7] A.-S. Bonnet-Ben Dhia, L. M. Faria, and C. Pérez-Arancibia. A complex-scaled boundary integral equation for time-harmonic water waves. *SIAM Journal on Applied Mathematics*, 84(4):1532–1556, 2024.
- [8] A.-S. Bonnet-Ben Dhia, B. Goursaud, and C. Hazard. Mathematical analysis of the junction of two acoustic open waveguides. *SIAM Journal on Applied Mathematics*, 71(6):2048–2071, 2011.
- [9] L. Bourgeois, S. Fliss, J.-F. Fritsch, C. Hazard, and A. Recoquilly. Scattering in a partially open waveguide: the forward problem. *IMA Journal of Applied Mathematics*, 88(1):102–151, 2023.
- [10] J. Bremer, Z. Gimbutas, and V. Rokhlin. A nonlinear optimization procedure for generalized Gaussian quadratures. *SIAM Journal on Scientific Computing*, 32(4):1761–1788, 2010.
- [11] O. P. Bruno, E. Garza, and C. Pérez-Arancibia. Windowed Green function method for nonuniform open-waveguide problems. *IEEE Transactions on Antennas and Propagation*, 65(9):4684–4692, 2017.
- [12] O. P. Bruno, M. Lyon, C. Pérez-Arancibia, and C. Turc. Windowed Green function method for layered-media scattering. *SIAM Journal on Applied Mathematics*, 76(5):1871–1898, 2016.



- [13] W. Cai. *Computational Methods for Electromagnetic Phenomena: electrostatics in solvation, scattering, and electron transport*. Cambridge University Press, 2013.
- [14] T. Christiansen. Scattering theory for perturbed stratified media. *Journal d'Analyse Mathématique*, 76(1):1–43, 1998.
- [15] S. Dyatlov and M. Zworski. *Mathematical Theory of Scattering Resonances*, volume 200 of *Graduate studies in mathematics*. American Mathematical Society, 2019.
- [16] C. L. Epstein. Solving the transmission problem for open waveguides, I fundamental solutions and integral equations. *arXiv preprint arXiv:2302.04353*, 2023.
- [17] C. L. Epstein. Solving the transmission problem for open waveguides, II outgoing estimates. *arXiv preprint arXiv:2310.05816*, 2023.
- [18] C. L. Epstein, L. Greengard, J. Hoskins, S. Jiang, and M. Rachh. Coordinate complexification for the Helmholtz equation with Dirichlet boundary conditions in a perturbed half-space. *arXiv preprint arXiv:2409.06988*, 2024.
- [19] C. L. Epstein and R. Mazzeo. Solving the scattering problem for open waveguides, III: Radiation conditions and uniqueness. *arXiv preprint arXiv:2401.04674*, 2024.
- [20] I. Good. The colleague matrix, a Chebyshev analogue of the companion matrix. *The Quarterly Journal of Mathematics*, 12(1):61–68, 1961.
- [21] G. R. Hadley. Transparent boundary condition for the beam propagation method. *IEEE Journal of Quantum Electronics*, 28(1):363–370, 1992.
- [22] K. L. Ho. FLAM: Fast linear algebra in MATLAB-algorithms for hierarchical matrices. *Journal of Open Source Software*, 5(51):1906, 2020.
- [23] J. Hoskins and M. Rachh. On the discretization of Laplace’s equation with neumann boundary conditions on polygonal domains. *Journal of Computational Physics: X*, 8:100072, 2020.
- [24] W. Huang and C. Xu. Simulation of three-dimensional optical waveguides by a full-vector beam propagation method. *IEEE journal of quantum electronics*, 29(10):2639–2649, 1993.
- [25] S. Jiang and V. Rokhlin. Second kind integral equations for the classical potential theory on open surfaces II. *Journal of Computational Physics*, 195(1):1–16, 2004.
- [26] S. Kim and H. Zhang. Optimized Schwarz method with complete radiation transmission conditions for the Helmholtz equation in waveguides. *SIAM Journal on Numerical Analysis*, 53(3):1537–1558, 2015.

- [27] M. Koshiba, Y. Tsuji, and S. Sasaki. High-performance absorbing boundary conditions for photonic crystal waveguide simulations. *IEEE Microwave and wireless components letters*, 11(4):152–154, 2001.
- [28] R. Kress. *Linear integral equations*. Springer, 1989.
- [29] W. Lu, Y. Y. Lu, and J. Qian. Perfectly matched layer boundary integral equation method for wave scattering in a layered medium. *SIAM Journal on Applied Mathematics*, 78(1):246–265, 2018.
- [30] P.-G. Martinsson. *Fast direct solvers for elliptic PDEs*. SIAM, 2019.
- [31] R. B. Melrose. Spectral and scattering theory for the Laplacian on asymptotically euclidian spaces. In *Spectral and scattering theory*, pages 85–130. CRC Press, 2020.
- [32] W. A. Mulder. Exact non-reflecting boundary conditions with an FDTD scheme for the scalar wave equation in waveguide problems. *Progress in Electromagnetics Research M*, 91:39–48, 2020.
- [33] V. I. Okhmatovski and A. C. Cangellaris. Evaluation of layered media Green’s functions via rational function fitting. *IEEE microwave and wireless components letters*, 14(1):22–24, 2004.
- [34] F. T. Orlandini, P. R. Devloo, and H. E. Hernández-Figueroa. A waveguide port boundary condition based on approximation space restriction for finite element analysis. *arXiv preprint arXiv:2407.21766*, 2024.
- [35] J. Ott. *Halfspace matching: a domain decomposition method for scattering by 2D open waveguides*. PhD thesis, Dissertation, Karlsruhe, Karlsruher Institut für Technologie (KIT), 2017, 2017.
- [36] M. Paulus, P. Gay-Balmaz, and O. J. Martin. Accurate and efficient computation of the Green’s tensor for stratified media. *Physical Review E*, 62(4):5797, 2000.
- [37] C. Pérez-Arancibia and O. P. Bruno. High-order integral equation methods for problems of scattering by bumps and cavities on half-planes. *JOSA A*, 31(8):1738–1746, 2014.
- [38] F. Santosa and R. Magnanini. Wave propagation in a 2-D optical waveguide. *SIAM Journal on Applied Mathematics*, 61(4):1237–1252, 2001.
- [39] J. Shibayama, M. Muraki, R. Takahashi, J. Yamauchi, and H. Nakano. Performance evaluation of several implicit FDTD methods for optical waveguide analyses. *Journal of lightwave technology*, 24(6):2465, 2006.
- [40] I. Sofronov, L. Dovgilevich, and N. Krasnov. Application of transparent boundary conditions to high-order finite-difference schemes for the wave equation in waveguides. *Applied Numerical Mathematics*, 93:195–205, 2015.

- [41] A. Tambova, S. P. Groth, J. K. White, and A. G. Polymeridis. Adiabatic absorbers in photonics simulations with the volume integral equation method. *Journal of Lightwave Technology*, 36(17):3765–3777, 2018.
- [42] G. Taraldsen. The complex image method. *Wave Motion*, 43(1):91–97, 2005.
- [43] A. Vasy. Structure of the resolvent for three-body potentials. *Duke Mathematical Journal*, 90(2):379, 1997.
- [44] A. Vasy. Propagation of singularities in three-body scattering. *Astérisque*, 262:158, 2000.
- [45] B. Wang, W. Zhang, and W. Cai. Fast multipole method for 3-D Helmholtz equation in layered media. *SIAM Journal on Scientific Computing*, 41(6):A3954–A3981, 2019.
- [46] Y. Wang, T. Goodwill, L. Greengard, J. Hoskins, and M. Rachh. Complexification for integral equations, ii. in preperation.
- [47] Y. Wang, T. Goodwill, L. Greengard, J. Hoskins, and M. Rachh. Fast multipole methods with complex coordinates. in preperation.
- [48] L. Zhang, J. H. Lee, A. Oskooi, A. Hochman, J. K. White, and S. G. Johnson. A novel boundary element method using surface conductive absorbers for full-wave analysis of 3-D nanophotonics. *Journal of Lightwave Technology*, 29(7):949–959, 2011.
- [49] W. Zhang, B. Wang, and W. Cai. Exponential convergence for multipole and local expansions and their translations for sources in layered media: Two-dimensional acoustic wave. *SIAM Journal on Numerical Analysis*, 58(3):1440–1468, 2020.